Dilatonic dynamics of baryonic crystals, branes, and spheres

Jahmall Bersini,[1,*] Alessandra D'Alise,[2,3,4,†] Francesco Sannino,[2,3,4,‡] and Matías Torres[2,3,5,§]

[1]*Kavli IPMU (WPI), UTIAS, The University of Tokyo, Kashiwa, Chiba 277-8583, Japan*
[2]*Department of Physics E. Pancini, Università di Napoli Federico II, via Cintia, 80126 Napoli, Italy*
[3]*INFN sezione di Napoli, via Cintia, 80126 Napoli, Italy*
[4]*Quantum Theory Center (ħQTC) at IMADA and D-IAS, Southern Denmark University, Campusvej 55, 5230 Odense M, Denmark*
[5]*Physique Théorique et Mathématique Université libre de Bruxelles and International Solvay Institutes, Campus Plaine C.P. 231, B-1050 Bruxelles, Belgium*

(Received 30 January 2024; accepted 22 September 2024; published 7 November 2024)

We systematically analyze the impact of dilatonic dynamics on Skyrme spheres, crystals, and branes. The effects of the dilatonic model parameters, encompassing different underlying near-conformal dynamics, on the macroscopic properties of skyrmions such as their mass and radius are discussed. For spheres and crystals we identify special values of the ratio of the decay constants for which the second order differential equations reduce to a solvable first order system. Additionally, in the case of the crystals, the dilaton presence spatially separates the baryon and isospin charge distributions. For branes, we show how the dilaton smooths out their configurations. Our results are expected to have wide implications from the study of near-conformal dynamics stemming from QCD-like theories to phenomenological investigations of nuclear matter in extreme regimes.

DOI: 10.1103/PhysRevD.110.094008

I. INTRODUCTION

Strong dynamics is notoriously hard to tackle both analytically and numerically. Over several decades, methodologies have been devised to access different dynamical regimes of strongly interacting theories. At sufficiently low energies, chiral Lagrangians have been shown to faithfully describe the dynamics of specific strongly coupled underlying theories in terms of their Goldstone bosons. This approach has landed precious information on the dynamics and spectrum of various models of which quantum chromodynamics (QCD) is the time-honored example. The approach is also routinely employed to inform (and extract information from) first principle numerical simulations. Another remarkable property of chiral Lagrangians is that their nonperturbative solutions describe extended objects that, depending on the boundary conditions (BCs), can be identified with distinct physical configurations, from crystals to branes and spheres. The spherical case (the hedgehog solution) is the oldest example dating back to the pioneering work of Skyrme [1]. Once the topological sector of the theory is taken into account [2,3], the properly quantized hedgehog solutions describe half-integer states with topological charge identified as the baryon number. These extended states are taken to be the nucleons of the underlying theory. Astonishingly, the same model can simultaneously describe mesonic degrees of freedom and their scattering properties, as well as the spectrum and form factors of extended baryonic states, including the Goldstone boson scattering off them. Therefore, the same effective Lagrangian coefficients control both the pion dynamics as well as the baryon spectrum and form factors. The operators of the chiral effective Lagrangian can be organized in the number of derivative and pion masses. The solitonic solutions can be mapped into baryon states of the underlying QCD-like dynamics at large number of colors. The dependence on the number of colors is naturally encoded in the pion decay constant and depends on the underlying fermion representation with respect to the asymptotically free gauge group. The Skyrme model has also been enriched by adding at the Lagrangian level massive vector mesons that have been shown to play an important role, not only to give a deeper understanding of the origin of the Skyrme term but also for the associated phenomenological consequences [4–7]. Finally, a less explored avenue that still deserves much attention, especially after the renewed experimental interest in heavy baryon spectroscopy and transitions [8–10], is the study of

*Contact author: jahmall.bersini@ipmu.jp
†Contact author: alessandra.dalise@unina.it
‡Contact author: sannino@qtc.sdu.dk
§Contact author: matiasignacio.torressandoval@unina.it

heavy baryons as bound states of a Skyrme soliton and heavy mesons [11–23]. The original idea pioneered by Callan and Klebanov [11] and first tailored for baryons made by one strange quark and two light quarks could, however, account only for half of the physical states possible in QCD. The issue was resolved analytically in [24] by consistently introducing excited heavy mesons. When working with heavy quarks such as the charm and the bottom ones, the approach hugely benefits from the marriage between large number of color dynamics and the celebrated heavy quark limit of QCD [25–31].

Beyond the traditional phenomenological nuclear and particle physics applications, here we systematically investigate the solitonic dynamics when the underlying gauge-fermion theory is near conformal. The region in the number of flavors versus the number of colors of asymptotically free gauge theories where the infrared theory is conformal is dubbed "conformal window." The phase diagram structure for QCD and QCD-like theories appeared in [32,33]. At the lower edge of the conformal window the theory undergoes a quantum phase transition from an infrared conformal field theory to a phase characterized by both conformal and chiral symmetry breaking [34,35]. When the transition is sufficiently smooth, close to the lower end of the conformal window, the theory exhibits a near-conformal phase characterized by the existence of a region of the renormalization group (RG) flow in which the coupling remains nearly constant signaling the occurrence of "walking dynamics" [36–38]. Walking behavior lies at the core of many phenomenological models of dynamical electroweak symmetry breaking, e.g., within the technicolor [32,33,38–43] and (fundamental partial) composite Goldstone Higgs scenarios [44–52].

The infrared dynamics of the near-conformal theory can be modeled by augmenting the standard chiral Lagrangian via the introduction of a new light scalar degree of freedom with the same quantum numbers of the vacuum which is commonly referred to as the "dilaton" or "radion." In this scenario, the dilaton is the Goldstone boson stemming from the spontaneous breaking of scale invariance, whereas sources of explicit conformal breaking leading to the near-conformal phase can be encoded in the effective dilaton potential. The aforementioned phenomenological applications have motivated several investigations of the resulting dilaton effective field theory (EFT) [42,53–69].

In this work, we present several classes of extended objects emerging as solitons of the dilaton augmented EFT. We identify crystal, brane, and sphere phases constituted, respectively, by ordered arrays of hadronic tubes, layers, and spherical hedgehog solitonic solutions at nonvanishing baryon number.

Until very recently, it was considered hard to construct analytical solutions representing baryonic condensates in the low-energy limit of QCD. However, in Refs. [70–77] an exact method to build hadronic solitons has been introduced. These solutions disclose intriguing nonperturbative features of the finite density phase diagram. For these reasons, it is very interesting to analyze what happens when the dilatonic degree of freedom is taken into account.

Skyrmions under the effects of dilaton dynamics have already been employed to describe dense nuclear matter such as the core of neutron stars [78–86]. In this framework, conformal invariance is seen as an emergent hidden symmetry of real-world QCD at high densities as suggested by both theoretical models and neutron star data [80,86–88]. Starting from the pioneering work of Brown and Rho [89], who introduced the dilaton mode to derive a series of scaling relations among the values of decay constants and masses in vacuum and at finite density, the dilaton EFT is considered to be a key ingredient for studying skyrmion matter in extreme conditions. These relations are shown to be modified when considering generalized EFTs [90]. While earlier works considered a simplified version of the effective action, the construction has later been refined in [91] and since then the dilaton EFT has become one of the building blocks of the generalized nuclear effective field theory, which aims at the description of hadronic matter from low to compact star densities (see, e.g., [92,93] for recent reviews). However, to the best of our knowledge, no comprehensive analysis of the spherical skyrmion properties in near-conformal theories has been performed.

The overarching goal of the present work is to combine numerical and analytical methods to perform a systematic investigation of skyrmion solutions in the presence of dilatonic dynamics. Applications range from the dynamics of QCD-like theories close to the lower end of the conformal window to nuclear matter in extreme regimes.

We structure our work as follows. After introducing the dilaton augmented EFT in Sec. II, we present a systematic numerical analysis in Sec. III. More specifically, we employ the standard hedgehog ansatz [2] and determine relevant physical quantities such as the skyrmion profile, mass, and size as a function of the physical parameters responsible for the deviations from conformal dynamics. Concretely, these are the anomalous dimension of the quark mass operator, the dilaton mass, and the conformal dimension of the relevant operator triggering the RG flow away from the infrared fixed point. We unveil an intricate dependence of the solitonic properties on these parameters as a consequence of the competition of dilaton and pion mass terms. We discover that the dilaton decouples rapidly from the dynamics once its mass exceeds the mass of the Goldstone modes. Moreover, we show that the dilaton decouples faster when the anomalous dimension of the chiral condensate is large.

We further show the existence of a special value of the ratio of dilaton and pion decay constants where the coupled second order field equations of the dilaton augmented EFT reduce to a first order solvable system. Therefore, the construction of analytic solitonic solutions is achieved

through the identification of a novel special point in the parameter space of the theory. Interestingly, such a point does not correspond to any bound on the energy. This is a surprising result since, without the dilaton, the field equations with the spherical hedgehog ansatz are not solvable. However, we find that the so-constructed solutions, which feature a negative topological charge $B=-1$, are singular at the origin and do not carry finite energy.

In Sec. IV, we study the impact of the dilaton on the skyrmion crystals investigated in [74–77]. After briefly reviewing the analytical solution in the absence of the dilaton, we show that even for the emerging hadronic tubes there exists a special parameter point where the coupled second order equation of motions (EOMs) reduce to a first order system [again without a Bogomol'nyi-Prasad-Sommerfield (BPS) bound on the energy]. The special parameter point is shown to be related to the one observed in the spherically symmetric case by mapping into each other the respective EOMs. We further notice that the presence of the dilaton spatially separates the baryon and isospin charge distributions similar to spin-charge separation discussed in [94,95].

Finally, it has been proposed that nuclear matter at low temperatures may exist in nonuniform branelike structures which may be realized in the crusts of neutron stars [96]. In fact, these configurations appear as ground states in numerical simulations where nucleons are treated as classical bodies with pairwise interactions (see, e.g., [97] for a recent review). Intriguingly, a class of analytic solutions of the Skyrme model describing solitonic brane configurations has been discovered in [70–73,77]. While it is tempting to identify these exact solutions with the results of the numerical studies, establishing a quantitative connection is not straightforward. In particular, a full quantization of the solitonic solutions appears to be extremely involved [73], and, therefore, their phenomenological relevance remains an interesting open problem that lies beyond the scope of the present work. Instead, inspired by the possible emergent scale symmetry in dense skyrmion matter, we study the impact of the dilaton on the analytic brane solutions in Sec. V. In particular, assuming that the fields depend at most on time and a single spatial coordinate, we find the general brane solution to the EOMs of the dilaton-dressed Skyrme model. We discover that, while the soliton profile is left unaltered by the presence of the dilaton, the latter acquires a homogeneous vacuum expectation value which is nontrivially determined by the soliton properties and the dilaton potential. For any given topological charge, we determine the lower bound on the dilaton mass such that the solutions exist. Finally, we discuss how the dilaton smooths out the brane structure at low values of the dilaton mass.

We offer our conclusion in Sec. VI. The Appendix summarizes our numerical results for the spherical skyrmion solutions in Tables I–VI.

II. DILATON DRESSING OF THE CHIRAL LAGRANGIAN

The Skyrme Lagrangian for $N_f=2$ massive flavors in four dimensions reads

$$I[U]=\int d^4x\sqrt{-g}\frac{K}{2}\mathrm{Tr}\left(\frac{1}{2}R_\mu R^\mu+\frac{\lambda}{16}F_{\mu\nu}F^{\mu\nu}+\frac{m_\pi^2}{2}(U+U^\dagger)\right), \tag{1}$$

$$R_\mu=U^{-1}\nabla_\mu U=R_\mu^j t_j, \qquad F_{\mu\nu}=[R_\mu,R_\nu]. \tag{2}$$

Here $U\in SU(2)$, ∇_μ is the covariant derivative, and $t_a=i\sigma_a$ are the generators of the $SU(2)$ algebra, being σ_a the Pauli matrices. Here m_π is the pion mass, while K is related to the meson decay constant via $f_\pi=\sqrt{K}$. The above theory can describe low-energy quantum chromodynamics or any other underlying quantum field theory featuring the same pattern of chiral symmetry breaking.

The theory admits a conserved topological current J_μ given by

$$J^\mu=\epsilon^{\mu\nu\lambda\rho}\mathrm{Tr}(R_\nu R_\lambda R_\rho). \tag{3}$$

Integrating the zero component of J^μ on a time-slice surface Σ we obtain the topological charge

$$B=\frac{1}{24\pi^2}\int_\Sigma \epsilon^{ijk}\mathrm{Tr}(R_iR_jR_k). \tag{4}$$

This quantity corresponds to the winding number associated with U and is interpreted as the baryon number. The classical equations of motion are obtained by performing the functional variation with respect to U, yielding

$$\nabla_\mu\left(R^\mu+\frac{\lambda}{4}[R_\nu,F^{\mu\nu}]\right)-\frac{m_\pi^2}{2}\left(U-U^\dagger\right)=0. \tag{5}$$

These correspond to a set of three nonlinear coupled partial differential equations (PDEs).

In this work, we explore the solitonic dynamics in a quasiconformal regime by adding to the action a dilatonic degree of freedom. The latter is introduced to restore conformal invariance at the action level and provide a mechanism for breaking conformality in a controllable manner. The pion mass term acts as an independent and controllable parameter for explicit conformal symmetry breaking. We, therefore, dress every operator O_k of mass dimension k with the dilaton field σ as [98,99]

$$O_k\to e^{(k-4)\sigma f}O_k, \tag{6}$$

where under a scale transformation $x\to e^\alpha x$ the field σ transforms as

$$\sigma \to \sigma - \frac{\alpha}{f}. \tag{7}$$

Here f is the length related to the spontaneous breaking of scale invariance. Possible sources of explicit conformal breaking can be modeled by perturbing the underlying conformal theory via

$$\delta L_{\mathcal{O}} = \lambda_{\mathcal{O}} \mathcal{O}, \tag{8}$$

with $\mathcal{O}$ an operator with dimension $\Delta \neq 4$ and $\lambda_{\mathcal{O}}$ the associated coupling. The presence of such an operator generates the following effective dilaton potential [65,66,68,99–101]:

$$V(\sigma) = f^{-4} e^{-4\sigma f} \sum_{n=0}^{\infty} c_n e^{-n(\Delta-4)f\sigma}, \tag{9}$$

where the coefficients c_n depend on the microscopic theory and scale as $c_n \sim \lambda_{\mathcal{O}}^n$ [66,68,99,101]. In the present work, we are interested in cases where the explicit conformal breaking is small which, in turn, can be realized when $\lambda_{\mathcal{O}} \ll 1$ and/or $\Delta \to 4$. In the first case, one can truncate the expansion (9) and obtain [61,66,68,99,101]

$$V(\sigma) = \frac{m_\sigma^2 e^{-4f\sigma}}{4(4-\Delta)f^2}\left(1 - \frac{4}{\Delta} e^{-(\Delta-4)f\sigma}\right) + \mathcal{O}(\lambda_{\mathcal{O}}^2), \tag{10}$$

where we introduced the dilaton mass m_σ and required that the ground state is realized for $\sigma = 0$. In the EFT spirit, the nature of the conformal breaking deformation and its conformal dimension Δ are left unspecified.[1] When $\Delta = 2$, Eq. (10) reduces to the usual ϕ^4 Higgs-like potential, whereas when Δ vanishes the coefficient c_1 becomes parametrically larger than c_0 and the potential (10) diverges. In Sec. III, we will conduct our numerical investigations in the range $1 \leq \Delta \leq 4$. On the other hand, by subtracting the infinite constant[2] appearing in the expansion of Eq. (10) around $\Delta = 0$, one obtains the dilaton potential considered in the classic work of Coleman [98],

$$V^{(2)}_{\Delta\to 0}(\sigma) = -\frac{m_\sigma^2}{16 f^2}(1 - 4f\sigma - e^{-4f\sigma}). \tag{11}$$

For the sake of completeness, we will also consider the traditional Coleman potential in the following analyses.

[1]The potential (10) has also been related to the gluon condensate $\langle G^2 \rangle$ and the usual soft dilaton theorems [61,68]. However, it has recently been argued that the only value of Δ consistent with the soft theorems is $\Delta = 2$ [102].

[2]The potential in (10) is strictly defined for any $\Delta > 0$. One way to derive the $\Delta = 0$ limit from (10) is to perform an *ad hoc* subtraction that depends on the underlying theory and yields (11). This subtraction, however, does not affect the equations of motion.

In the limit $\Delta \to 4$ we have that $\mathcal{O}$ becomes a near marginal operator and it is legitimate to expand Eq. (9) in powers of $\Delta - 4$ as

$$V(\sigma) = -\frac{m_\sigma^2 e^{-4f\sigma}}{16 f^2}(1 + 4f\sigma) + \mathcal{O}\big((\Delta-4)^2\big). \tag{12}$$

The form of the potential in (12) agrees with the counting scheme proposed in [57,58,60,62,64]. Moreover, at the considered order in the EFT expansion, Eq. (12) coincides with the potential derived in [67] starting from the partially conserved dilatation current relation and has often been employed to describe dense skyrmion matter, see, e.g., [78,79,82,85,89]. Crucially, since Eq. (12) can be seen as a subcase (the $\Delta \to 4$ limit) of Eq. (10), in this work we will consider the generic form of the dilaton potential appearing in Eq. (10) to encompass all the proposals considered in the literature so as to keep our analysis as general as possible without committing to a specific model.

We can now also take into account the explicit breaking of conformal symmetry stemming from the presence of quark masses. We achieve this by assuming the mass term to have dimension $y = 3 - \gamma$, where $0 < \gamma < 2$ is the anomalous dimension of the chiral condensate and its range is limited by the unitarity bound. Moreover, since for $\gamma \simeq 1$ the underlying four-fermion operator becomes nearly marginal, we will focus on the interval $0 < \gamma < 1$.

We, therefore, arrive at the following dilaton augmented chiral Lagrangian:

$$\begin{aligned} I[U,\sigma] = \int d^4x\sqrt{-g}\Big[\frac{K}{2}\mathrm{Tr}\Big(&\frac{1}{2}R^\mu R_\mu e^{-2\sigma f} \\ &+ \frac{\lambda}{16}F_{\mu\nu}F^{\mu\nu} + \frac{m_\pi^2}{2}(U+U^\dagger)e^{-y\sigma f}\Big) \\ &- \frac{1}{2}e^{-2\sigma f}\nabla_\mu\sigma\nabla^\mu\sigma - V(\sigma)\Big]. \end{aligned} \tag{13}$$

Although we restricted the number of flavors to two, we stress that conformality can be realized with such a small number of flavors in a number of theories, such as the ones with fermions in the two index symmetric or antisymmetric representation of the gauge group as shown first in [32] and generalized in [33]. In any case, here we focus on the impact of the novel dilatonic dynamics on time-honored solitons first discussed for the two and three flavor cases.

In order to investigate these extended objects, one starts with the equations of motion that read

$$\nabla_\mu\left(R^\mu e^{-2\sigma f} + \frac{\lambda}{4}[R_\nu, F^{\mu\nu}]\right) - \frac{m_\pi^2}{2}(U - U^\dagger)e^{-y\sigma f} = 0, \tag{14}$$

$$\begin{aligned} &\nabla_\mu\left(e^{-2\sigma f}\nabla^\mu\sigma\right) + f\nabla^\mu\sigma\nabla_\mu\sigma e^{-2\sigma f} - \partial_\sigma V(\sigma) \\ &-\frac{K}{2}f\mathrm{Tr}R_\mu R^\mu e^{-2\sigma f} - \frac{K}{4}yfm_\pi^2\mathrm{Tr}\left(U+U^\dagger\right)e^{-y\sigma f} = 0, \end{aligned} \tag{15}$$

while the stress-energy tensor $T_{\mu\nu} = -\frac{2}{\sqrt{-g}}\frac{\partial\sqrt{-g}\mathcal{L}}{\partial g^{\mu\nu}}$ is given by

$$\begin{aligned} T_{\mu\nu} = &-\frac{K}{2}\mathrm{Tr}\left[\left(R_\mu R_\nu - \frac{1}{2}g_{\mu\nu}R_\alpha R^\alpha\right)e^{-2\sigma f}\right. \\ &+\frac{\lambda}{4}\left(g^{\alpha\beta}F_{\mu\alpha}F_{\nu\beta} - \frac{1}{4}g_{\mu\nu}F_{\alpha\beta}F^{\alpha\beta}\right) \\ &\left.-\frac{m_\pi^2}{2}g_{\mu\nu}\left(U+U^\dagger\right)e^{-y\sigma f}\right] \\ &-\left(-\nabla_\mu\sigma\nabla_\nu\sigma + \frac{1}{2}g_{\mu\nu}(\nabla\sigma)^2\right)e^{-2\sigma f} - g_{\mu\nu}V(\sigma). \end{aligned} \tag{16}$$

The presence of the mass term shifts the value of the minimum of the dilaton potential from $\sigma = 0$ to a finite value that we indicate with $\langle\sigma\rangle = \sigma_f$. The latter is determined by the following equation:

$$\partial_\sigma V(\sigma)|_{\sigma=\sigma_f} + Kyfm_\pi^2 e^{-yf\sigma_f} = 0. \tag{17}$$

This leads to new values for the decay constants and the masses of all the states appearing in the Lagrangian satisfying certain scaling relations [62,64–66]. Equipped with the above, we are now ready to investigate several classes of solitonic configurations starting with the celebrated hedgehog solution.

III. DILATON AUGMENTED HEDGEHOG SKYRMIONS

A. Setup

In this section, we investigate the modification to the time-honored hedgehog solution in the presence of dilatonic dynamics. Let us start with a general parametrization for $U(x)$,

$$\begin{aligned} &U^{\pm1}(x^\mu) = \cos(\alpha)\mathbb{1}_{2\times2} \pm \sin(\alpha)n^a t_a, \\ &\quad n^1 = \sin(\Theta)\cos(\Phi), \quad n^2 = \sin(\Theta)\sin(\Phi), \\ &\quad n^3 = \cos(\Theta), \end{aligned} \tag{18}$$

where $\mathbb{1}_{2\times2}$ is the 2×2 identity matrix and $\alpha(x)$, $\Theta(x)$, and $\Phi(x)$ are the three scalar degrees of freedom of $SU(2)$. The hedgehog ansatz for $SU(2)$ in spherical coordinates $\{r,\theta,\phi\}$ reads

$$\alpha = \alpha(r), \quad \Theta = \theta, \quad \Phi = \phi. \tag{19}$$

The energy and topological charge densities are, respectively, given by

$$\begin{aligned} \epsilon = T_{00} = &\frac{1}{2}e^{-2f\sigma}\left(\frac{2K\sin^2(\alpha)}{r^2} + K\alpha'^2 + \sigma'^2\right) + \frac{\lambda K\alpha'^2\sin^2(\alpha)}{r^2} \\ &+\frac{\lambda K\sin^4(\alpha)}{2r^4} - Km_\pi^2\cos(\alpha)e^{-fy\sigma} + V(\sigma), \end{aligned} \tag{20}$$

$$\rho_B = J^0 = -\frac{12\alpha'\sin^2(\alpha)}{r^2}, \tag{21}$$

where the prime denotes the derivative with respect to the radial coordinate. The baryon mass M_S and charge B are, respectively, obtained by integrating the energy and charge densities of the solution over the whole spacetime, that is

$$M_s = 4\pi\int_0^\infty r^2\epsilon dr, \quad B = \frac{1}{6\pi}\int_0^\infty r^2\rho_B dr. \tag{22}$$

A measure of the size of the solitonic object is given by the root-mean-square radius of the baryon charge $\langle r^2\rangle^{1/2}$ defined as

$$\langle r^2\rangle^{1/2} \equiv \left(\frac{1}{6\pi}\int_0^\infty \rho_B r^4 \mathrm{d}r\right)^{1/2} = \sqrt{-\frac{2}{\pi}\int_0^\infty r^2\sin^2(\alpha)\alpha' dr}. \tag{23}$$

Inserting the hedgehog ansatz in (5) and (15) we obtain the following set of coupled second order differential equations:

$$\begin{aligned} &(2\lambda e^{2f\sigma}\sin^2(\alpha) + r^2)\alpha'' - 2r\alpha'(fr\sigma' - 1) \\ &\quad + \frac{\lambda e^{2f\sigma}\sin(2\alpha)(r^2\alpha'^2 - \sin^2(\alpha))}{r^2} - \sin(2\alpha) \\ &\quad - m_\pi^2 r^2\sin(\alpha)e^{-f(y-2)\sigma} = 0, \end{aligned} \tag{24}$$

$$\begin{aligned} &\sigma'' - f\sigma'^2 + \frac{2}{r}\sigma' - e^{2f\sigma}\partial_\sigma V(\sigma) + fK\alpha'^2 \\ &\quad + \frac{2}{r^2}fK\sin^2(\alpha) - Kfm_\pi^2 y\cos(\alpha)e^{f(2-y)\sigma} = 0. \end{aligned} \tag{25}$$

In the next section, we will numerically solve the above equations to investigate the dependence of the skyrmion properties on the parameters Δ, m_σ, y encoding the explicit breaking of conformal invariance.

B. Numerical solutions

To study the impact of dilatonic dynamics, we numerically solve the EOMs (24) and (25) in the sector of topological charge $B = 1$. We measure all the dimensionful quantities in units of $\sqrt{K}$ (in QCD $\sqrt{K} = 93$ MeV) and as a starting point we consider the following QCD-inspired values [2,66,78]:

$$f = 0.29, \quad \lambda = \frac{1}{4.75^2}, \quad m_\pi = \frac{140}{93}. \tag{26}$$

We then solve the EOMs for different values of the parameters Δ, m_σ, y. In particular, we consider $m_\sigma = 1, 2, \ldots, 10$ and $\Delta = 1, 1.2, 1.4, \ldots, 3.8$. Moreover, we study the limiting cases $\Delta \to 4$ and $\Delta \to 0$ corresponding

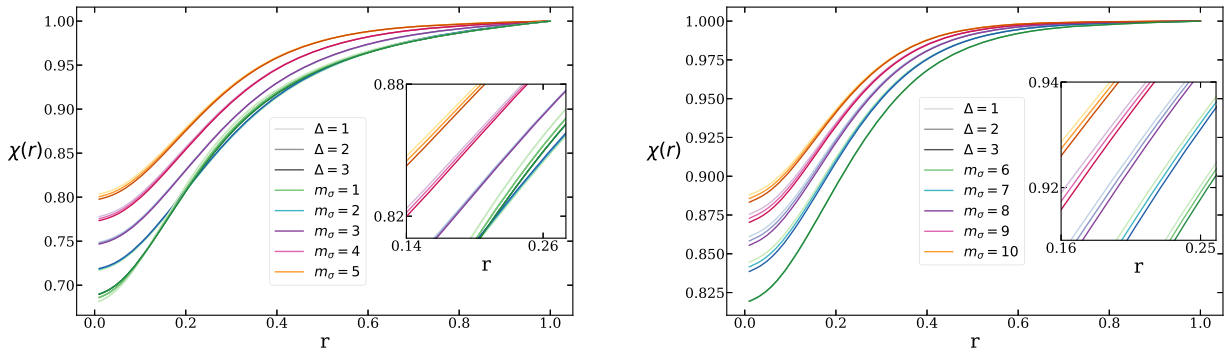

FIG. 1. Dilaton profile $\chi(r)$ for $\Delta = 1$–3 and $m_\sigma = 1$–5 (left) and $m_\sigma = 6$–10 (right).

to the dilaton potentials (12) and (11), respectively. For every value of Δ and m_σ, we determine the profile functions $\alpha(r)$ and $\sigma(r)$, the baryon mass M_S, and the root-mean-square radius of the baryon charge $\langle r^2\rangle^{1/2}$. Since the topologically trivial vacuum exhibits a divergent zero-point energy, we define M_S as the energy difference between the solutions with $B = 1$ and $B = 0$. To simplify the presentation, we momentarily set $y = 5/2$ and postpone to Sec. III B 2 the discussion of the dependence on the anomalous dimension of the chiral condensate. However, as we shall see, all the conclusions below apply to any value of y in the range $2 < y < 3$.

To set the boundary conditions, we impose that for $r \to \infty$ the fields approach the topologically trivial vacuum. We recall that at fixed values of time, the field $U(r)$ defines a map from the spatial manifold $\mathbb{R}^3$ to the isospin manifold S^3 with the boundary condition that $U(r)$ goes to its trivial vacuum for asymptotically large distances. In other words, we have

$$U(r \to \infty) = \mathbb{1} \Rightarrow \alpha(r \to \infty) = 0,$$
$$U(0) = -\mathbb{1} \Rightarrow \alpha(0) = \pi, \tag{27}$$

where the latter condition fixes the baryon charge to unity [2]. Analogously, we impose $\sigma(r \to \infty) \to \sigma_f$ with σ_f given in Eq. (17). Since σ_f depends on the values of the parameters we vary, this can be seen as a fixed BC for the normalized variable

$$\chi(r) \equiv e^{-f(\sigma(r)-\sigma_f)}, \tag{28}$$

namely, $\chi(r \to \infty) \to 1$. We note that one of the main differences with respect to earlier numerical studies [78,79] is that we do consider the dependence of σ_f on the pion mass. Finally, we impose $\chi'(0) = 0$ in line with previous investigations [78,79].

We study the dilaton potential (10) for $1 \leq \Delta < 4$ and its $\Delta \to 4$ limit (12) for $\Delta = 4$. We do not consider values of Δ smaller than 1 being the potential (10) ill defined in the $\Delta \to 0$ limit.

Figure 1 shows the dilaton profile $\chi(r)$ for $\Delta = 1$–3 and $m_\sigma = 1, \ldots, 10$. The general trend displayed in the figures can be summarized as follows.

(1) At fixed Δ the dilaton profile flattens toward its asymptotic value $\chi = 1$ as m_σ increases.[3]
(2) At fixed m_σ the dilaton profile flattens toward its asymptotic value $\chi = 1$ as Δ decreases.

The profile $\alpha(r)/\pi$ is depicted in Fig. 2 for the same choice of the parameters. As m_σ increases, the dilaton decouples from the dynamics and $\alpha(r)$ converges rapidly to the solution obtained in the absence of the dilaton. In general, the solutions exhibit little dependence on Δ.

Our results for M_S are collected in Appendix A 1 and illustrated in Fig. 3 for $m_\sigma = 3, 5, 7, 10$. For all the values of the parameters, the relative numerical error is less than 0.5%, where such a value should be seen as a conservative upper limit. One can see that at fixed values of m_σ the baryon mass gets smaller as Δ increases. On the other hand, the dependence of M_S on m_σ at fixed Δ is not monotonic. In fact, M_S first decreases with increasing m_σ until it reaches its minimum for $m_\sigma \sim 5$, after which it climbs toward its Skyrme model value $M_{\text{Skyrme}} = 15.67$. This behavior is illustrated in Fig. 4. A change in the behavior of the solutions around $m_\sigma = 5$ can be also seen by analyzing the values of $\langle r^2\rangle^{1/2}$, which are given in Tables II and IV in Appendix A 1. In fact, $\langle r^2\rangle^{1/2}$ increases with increasing m_σ until $m_\sigma \sim 5$ and then starts getting smaller for higher values of the dilaton mass. Moreover, while $\langle r^2\rangle^{1/2}$ grows monotonically with Δ for $m_\sigma = 1, 2, \ldots, 5, 6$, the opposite holds for $m_\sigma = 7$–10 as can be seen from Fig. 3.[4]

Finally, it is important to stress that the dependence of the skyrmion properties on both Δ and m_σ becomes quickly milder as we increase m_σ, implying that the dilaton decouples rapidly from the dynamics once its mass exceeds m_π. For instance, while for $m_\sigma = 1$ both M_S and $\langle r^2\rangle^{1/2}$

[3]The case $m_\sigma = 1$ constitutes an exception, since in this case the dilaton profile stays below the one obtained for $m_\sigma = 2$ only for small values of the radius.

[4]However, for $m_\sigma = 6$, the root-mean-square radius shows almost no dependence on Δ.

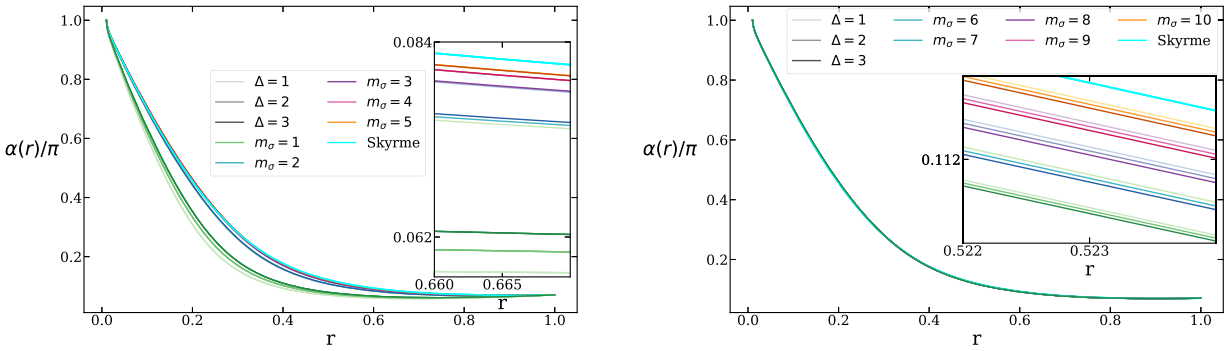

FIG. 2. Skyrmion profile $\alpha(r)$ for $\Delta = 1$–3 and $m_\sigma = 1$–5 (left) and $m_\sigma = 6$–10 (right).

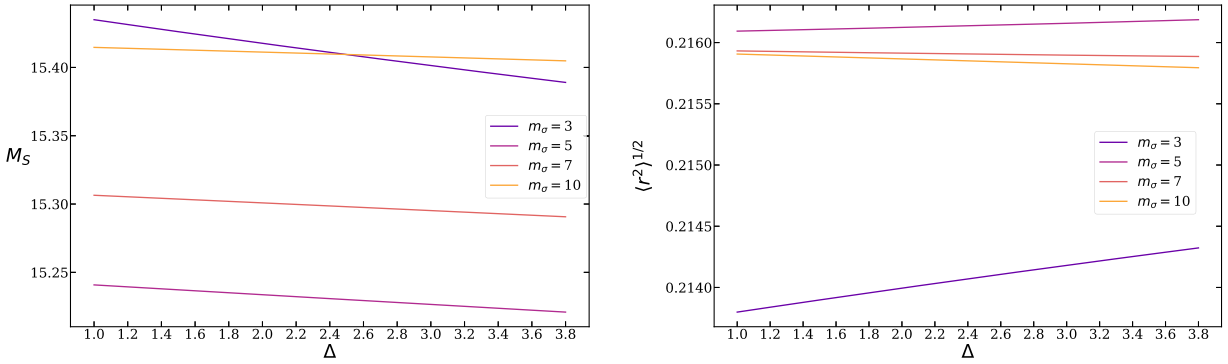

FIG. 3. M_S (left) and $\langle r^2\rangle^{1/2}$ (right) as a function of Δ for $m_\sigma = 3$, 5, 7, 10.

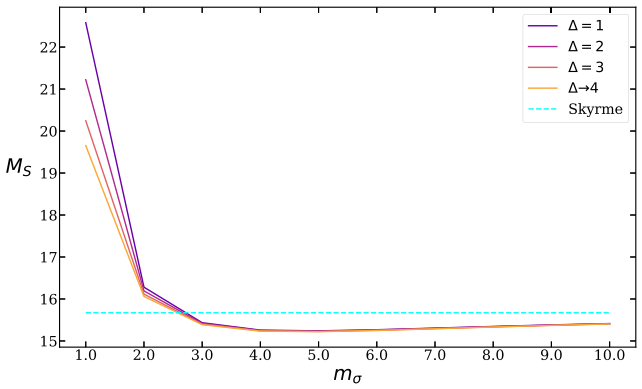

FIG. 4. The skyrmion mass M_S as a function of the dilaton mass m_σ for $\Delta = 1$ (purple), $\Delta = 2$ (red), $\Delta = 3$ (orange), and $\Delta = 4$ (yellow). The dashed line marks the value of the skyrmion mass in the absence of the dilaton ($M_{\text{Skyrme}} = 15.67$ in units of $\sqrt{K}$).

differ more than 20% from their values in the absence of the dilaton, such a difference reduces to less than 3% for $m_\sigma \geq 3$.

1. Skyrmions in the $\Delta \to 0$ limit

As previously discussed, the potential (10) diverges in the $\Delta \to 0$ limit. For completeness, we now discuss the solitonic solution in the presence of the potential (11), which can be seen as a regularized version of the $\Delta = 0$ case. To this end, we use the values of the parameters considered in the previous section.

The profiles of the fields are displayed in Fig. 5. Their behavior as we vary m_σ is similar to the one discussed in the $1 \leq \Delta \leq 4$ case with the dilaton profile becoming more flat and converging faster to $\chi = 1$ as m_σ increases, while $\alpha(r)$ converges quickly to the Skyrme model profile. However, note the exception in the dilaton profile for small values of m_σ, with the $m_\sigma = 1$ profile staying below the $m_\sigma = 2$ one only for small values of r. The behavior of the skyrmion mass and the root-mean-square radius as a function of m_σ is illustrated in Fig. 6 and mimics the one found in the previous section. In fact, M_S decreases, reaches its minimum around $m_\sigma \sim 5$, and then grows toward the Skyrme model value. At the same time, $\langle r^2\rangle^{1/2}$ mirrors such a behavior. Our results for M_S and $\langle r^2\rangle^{1/2}$ are listed in Appendix A 2.

2. The role of the anomalous dimension of the chiral condensate

The time is ripe to discuss the impact of the anomalous dimension of the chiral condensate on the skyrmion properties, i.e., the dependence on y. First, we note that all the conclusions drawn for the $y = 5/2$ case in the previous sections hold for every $2 < y < 3$. The dilaton

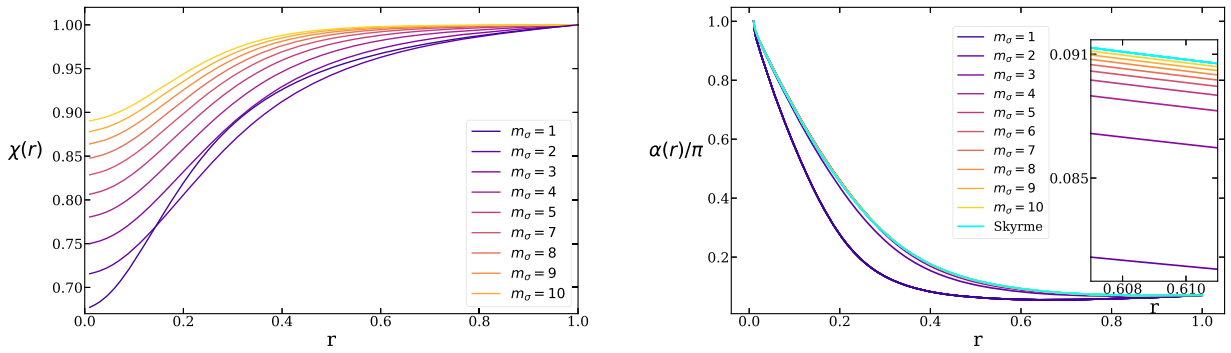

FIG. 5. Dilaton profile $\chi(r)$ (left) and $\alpha(r)/\pi$ (right) for the dilaton potential (11) and $m_\sigma = 1$–10.

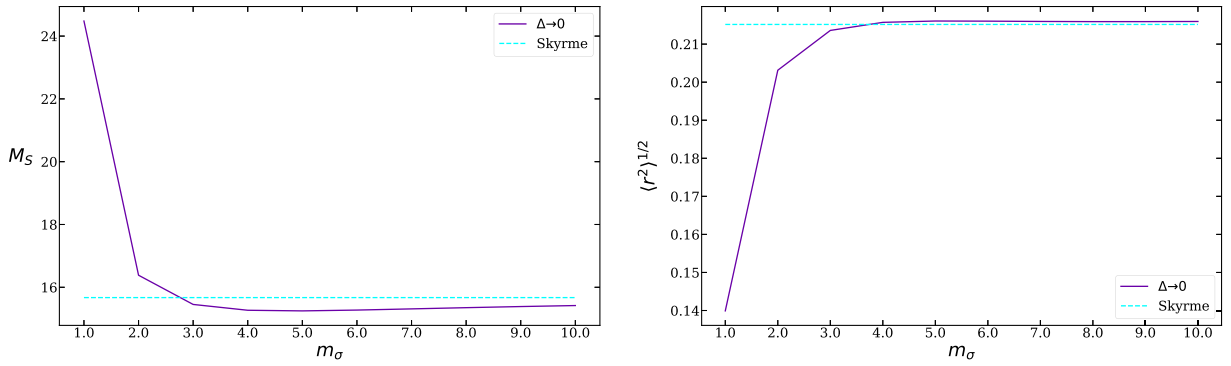

FIG. 6. The skyrmion mass M_S (left) and $\langle r^2\rangle^{1/2}$ (right) as a function of the dilaton mass m_σ. The dashed line marks the values obtained in the absence of the dilaton $M_{\text{Skyrme}} = 15.67$ and $\langle r^2\rangle^{1/2}_{\text{Skyrme}} = 0.215$.

profile $\chi(r)$ becomes flatter and converges earlier to its asymptotic value as y decreases. At the same time, the skyrmion profile $\alpha(r)$ approaches the profile in the absence of the dilaton as y decreases, signaling the decoupling of $\sigma(r)$ from the dynamics. To illustrate this behavior, we show the profiles obtained for $\Delta = 1$ and $m_\sigma = 2$ and different values of y in Fig. 7.

M_S and $\langle r^2\rangle^{1/2}$ get, respectively, larger and smaller as y varies from $y = 2$ to $y = 3$, as shown in Fig. 8. Moreover, the dependence on y gets weaker as the dilaton decouples for larger m_σ. Finally, our results for M_S and $\langle r^2\rangle^{1/2}$ confirm that the dilaton decouples faster for smaller y. For instance, this can be seen by looking at how the dependence of M_S (and $\langle r^2\rangle^{1/2}$) on both Δ and m_σ becomes softer as y decreases. This last point is exemplified in Fig. 9.

3. Numerical solutions in the chiral limit

We conclude our numerical analysis with a brief discussion of the solitonic solution in the chiral limit $m_\pi = 0$. Here the topological trivial vacuum state occurs for $U = \mathbb{1}$ and $\sigma = 0$. Therefore, the BC for $\chi(r)$ at infinity no longer depends on the value of m_σ and Δ. Keeping the same numerical values adopted in Sec. III B we solve the EOMs for $\Delta = 1, 1.2, \ldots, 4$ and $m_\sigma = 0$–4. The first observation is that all the solitonic properties are nearly independent on Δ for any value of m_σ. This is a direct consequence of the fact that the dilaton ground state value vanishes for any Δ. The dilaton $\chi(r)$ and $\alpha(r)/\pi$ profiles are displayed in Fig. 10 for $\Delta = 1$ and $m_\sigma = 0$–4. Analogously to $m_\pi \neq 0$ case, the dilaton profile progressively flattens as we increase its mass, exhibiting a faster convergence to unity. At the same time, the associated $\alpha(r)/\pi$ profile shows almost no dependence on m_σ. The baryon mass M_S is shown in Fig. 11. The dependence on Δ is similar (M_S gets smaller as Δ increases) but much weaker than in the $m_\pi \neq 0$ case for all values of m_σ. For instance, for $m_\sigma = 1$ the relative variation of the solitonic mass along the whole range of values of Δ is only ∼0.07%, to be compared with ∼15% obtained for $m_\pi = 140/93$ in Sec. III B. Moreover, the dependence on m_σ of both M_S and $\langle r^2\rangle^{1/2}$ is such that now the solitonic mass increases and the radius decreases toward the dilaton-decoupled limit as shown in Fig. 12. In the case of a nonvanishing m_π, it is the solitonic mass that decreases while the radius increases.

C. Analytical solution in the massless case

In the case of the chiral Lagrangian alone, the spherical hedgehog ansatz leads to a differential equation that can

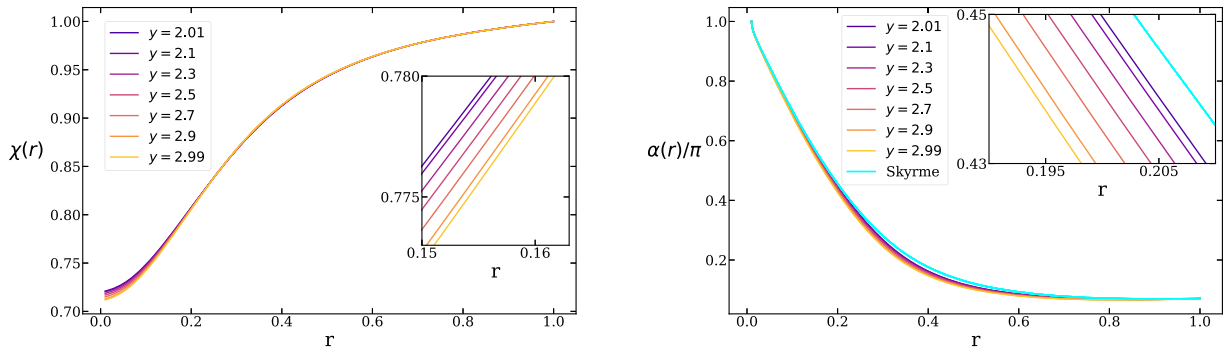

FIG. 7. Dilaton profile $\chi(r)$ (left) and $\alpha(r)/\pi$ (right) for $m_\sigma = 2$ and $\Delta = 1$.

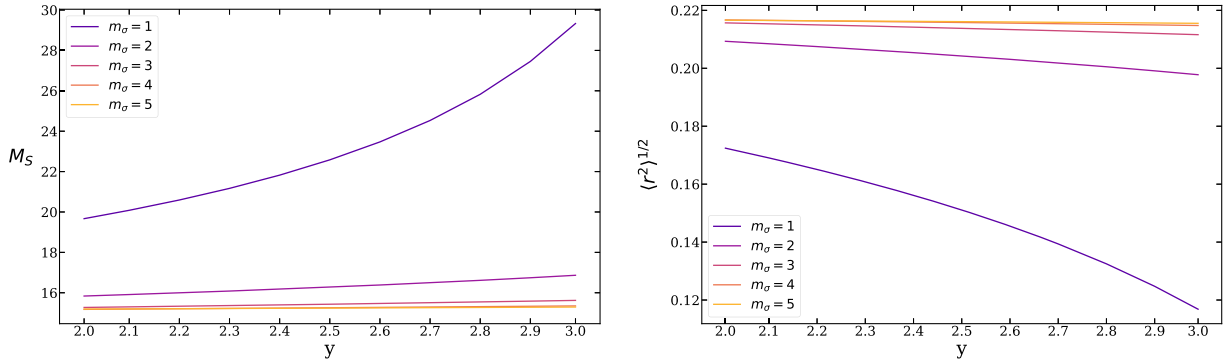

FIG. 8. M_S (left) and $\langle r^2 \rangle^{1/2}$ (right) as a function of y for $\Delta = 1$ and $m_\sigma = 1$–5.

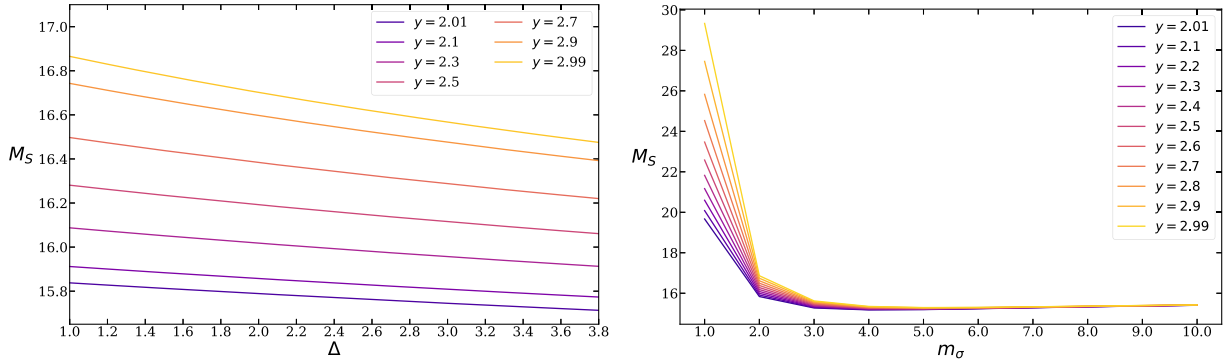

FIG. 9. The skyrmion mass M_S as a function of Δ for $m_\sigma = 2$ and $y = 2.01, 2.1, 2.3, 2.5, 2.7, 2.9, 2.99$ (left) and as a function of m_σ for $\Delta = 1$ and $y = 2.01, 2.1, 2.3, 2.5, 2.7, 2.9, 2.99$ (right).

only be solved using numerical methods. Quite remarkably, when the coupling with the dilaton is not neglected, it is possible to find an analytical solution for a special value of the couplings f and K due to an interesting phenomenon, namely, "BPS-like equations without a BPS bound." In fact, when $f^2K = 7/8$, the second order field equations can be reduced to a first order system even though there is no BPS bound on the energy of the system. The equations of motion (14) and (15) in the absence of mass and Skyrme term reduce to two nonlinear coupled ordinary differential equations (ODEs)

$$r^2\alpha'' - 2r\alpha'(fr\sigma' - 1) - \sin(2\alpha) = 0, \quad (29)$$

$$r^2\sigma'' + r(fKr\alpha'^2 + \sigma'(2 - fr\sigma')) + 2fK\sin^2(\alpha) = 0. \quad (30)$$

For later convenience, we change variables as $\rho = \log r$ and $\frac{\partial\sigma}{\partial\rho} \to \frac{\partial\sigma}{\partial\rho} + \frac{1}{2f}$ and rewrite the EOMs as

$$\ddot{\alpha} - 2f\dot{\alpha}\dot{\sigma} - \sin(2\alpha) = 0, \quad (31)$$

$$\ddot{\sigma} - f\dot{\sigma}^2 + fK\dot{\alpha}^2 + 2fK\sin^2(\alpha) + \frac{1}{4f} = 0, \quad (32)$$

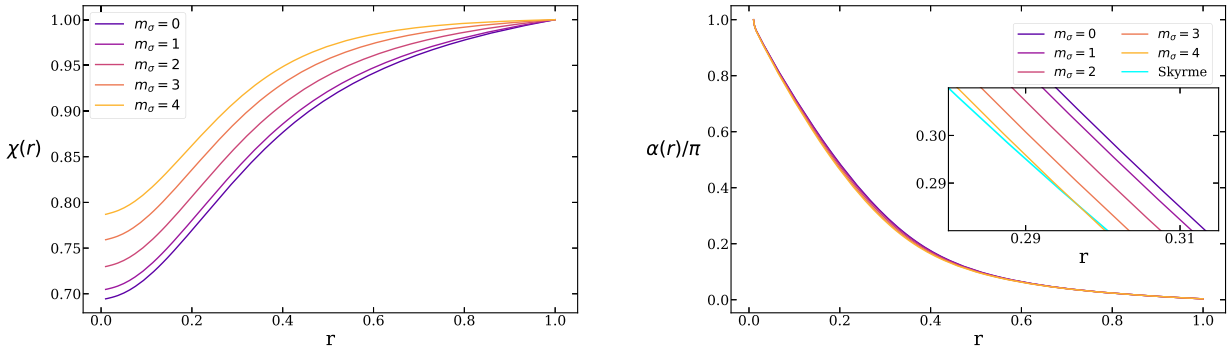

FIG. 10. Dilaton $\chi(r)$ (left) and $\alpha(r)/\pi$ (right) profiles for $\Delta = 1$ and $m_\sigma = 0$–4.

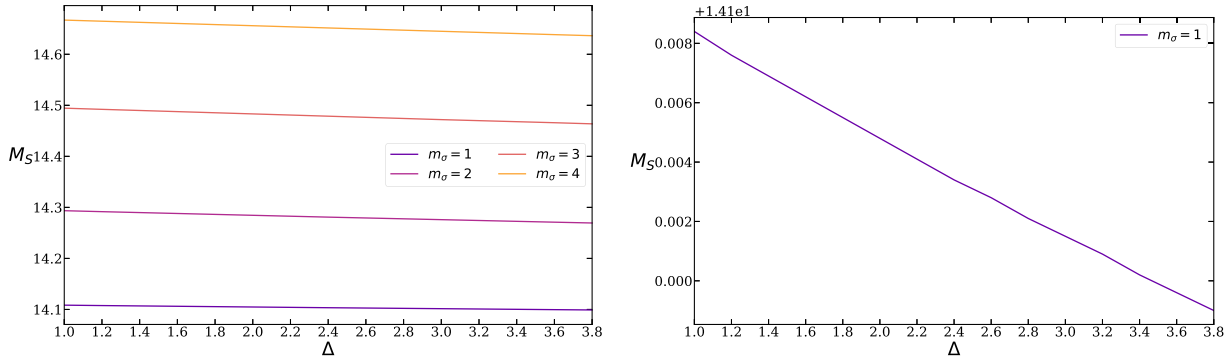

FIG. 11. Skyrmion mass M_S as a function of Δ for $m_\sigma = 1$–4 (left) and a detail of the $m_\sigma = 1$ line (right).

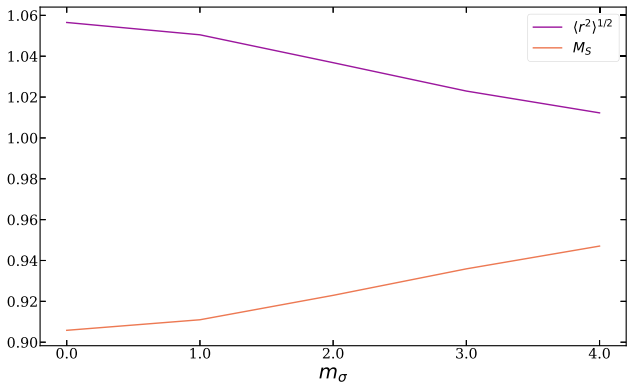

FIG. 12. Skyrmion mass M_S and root-mean-square radius $\langle r^2 \rangle^{1/2}$ normalized at their values in the absence of the dilaton ($M_{\text{Skyrme}} = 15.49$ and $\langle r^2 \rangle^{1/2}_{\text{Skyrme}} = 0.213$) as a function of m_σ.

where the dot denotes the derivative with respect to ρ. Noticeably, when $f^2 K = \frac{7}{8}$ we can find a first order system implying the EOMs,

$$\alpha' = \frac{\sqrt{2}}{r}\cos(\alpha), \tag{33}$$

$$\sigma' = -\frac{\sqrt{2}}{fr}\sin(\alpha) + \frac{1}{2fr}. \tag{34}$$

We can therefore solve for the analytical solution of the EOMs that read

$$\alpha_\pm(r) = n\pi + 2\tan^{-1}\left(1 - \frac{2c_1}{c_1 \pm (\frac{r}{r_0})^{\sqrt{2}}}\right), \quad n \in \mathbb{Z}, \tag{35}$$

$$\sigma_\pm(r) = \frac{1}{f}\left\{c_2 + \frac{1}{2}\log\left(\frac{r}{r_0}\right) + \log\left[\cos\left(2\tan^{-1}\left(1 - \frac{2c_1}{c_1 \pm (\frac{r}{r_0})^{\sqrt{2}}}\right)\right)\right]\right\}, \tag{36}$$

where the plus and minus signs apply for $c_1 > 0$ and $c_1 < 0$, respectively. The topological charge associated with this solution is $B = -1$. Conventional solitonic solutions of the chiral Lagrangian with negative winding numbers are called "antiskyrmions." The energy density of the solution reads

$$\epsilon = \frac{e^{-2c_2}}{8c_1^2 f^2 r^2}\left(\frac{r}{r_0}\right)^{-2\sqrt{2}-1}\left[(\sqrt{2}+4)c_1^4 - (\sqrt{2}-4)\left(\frac{r}{r_0}\right)^{4\sqrt{2}}\right] \tag{37}$$

and diverges at the origin as $r^{-2\sqrt{2}-3}$ due to the dilaton profile $\chi(r)$ being singular in $r=0$. Moreover, even excluding the singularity at $r=0$, the total energy would still diverge since the energy density does not decrease fast enough at large r.

IV. DILATON AUGMENTED CRYSTALS

In this section, we first review the strategies to find analytical solutions describing arrays of tubes of baryons with nontrivial topological charge on flat spacetime [74–77] and then we will generalize the solutions in the presence of the dilaton. The qualitative behavior of these exact solutions suggests they may be relevant for describing nuclear pasta states [96,97].

A. Crystals without the dilaton

We consider the action (2) in the absence of the Skyrme and mass terms and retain the same general parametrization for $U(x)$ given in (18). The equations of motion (5) constitute the following set of three nonlinear coupled PDEs,

$$-\Box\alpha+\sin(\alpha)\cos(\alpha)(\nabla_\mu\Theta\nabla^\mu\Theta+\sin^2(\Theta)\nabla_\mu\Phi\nabla^\mu\Phi)=0, \tag{38}$$

$$\sin^2(\alpha)\Box\Theta+2\sin(\alpha)\cos(\alpha)\nabla_\mu\alpha\nabla^\mu\Theta - \sin^2(\alpha)\sin(\Theta)\cos(\Theta)\nabla_\mu\Phi\nabla^\mu\Phi=0, \tag{39}$$

$$\sin^2(\alpha)\sin^2(\Theta)\Box\Phi+2\sin(\alpha)\cos(\alpha)\sin^2(\Theta)\nabla_\mu\alpha\nabla^\mu\Phi + 2\sin^2(\alpha)\sin(\Theta)\cos(\Theta)\nabla_\mu\Theta\nabla^\mu\Phi=0, \tag{40}$$

where we have not yet made any ansatz for the parameters of U in terms of the coordinates. Here the topological charge density $\rho_B\equiv J^0$ takes the following form:

$$\rho_B=12\sin^2(\alpha)\sin(\Theta)d\alpha\wedge d\Theta\wedge d\Phi. \tag{41}$$

From this expression, we observe that in order to have $d\alpha\wedge d\Theta\wedge d\Phi\neq 0$ the fields α, Θ, and Φ must be independent. Additionally, in order to decouple the previous set of equations, we impose

$$\nabla_\mu\Phi\nabla^\mu\alpha=\nabla_\mu\alpha\nabla^\mu\Theta=\nabla_\mu\Phi\nabla^\mu\Phi=\nabla_\mu\Theta\nabla^\mu\Phi=0. \tag{42}$$

We proceed by confining the system into a box described by the following line element:

$$ds^2=-dt^2+L_x^2dx^2+L_y^2dy^2+L_z^2dz^2, \tag{43}$$

where $\{x,y,z\}$ are dimensionless coordinates having the range

$$0\le x\le 2\pi,\quad 0\le y\le\pi,\quad 0\le z\le 2\pi. \tag{44}$$

The condition (42) is then realized by considering the following ansatz:

$$\alpha=\alpha(x),\quad \Theta=qy,\quad \Phi=p\left(\frac{t}{L_z}-z\right),\qquad q=2v+1,\quad v,p\in\mathbb{Z}, \tag{45}$$

such that the equations of motion reduce to a single integrable ODE for the profile $\alpha(x)$,

$$\partial_x\left[\frac{1}{2}(\alpha')^2-V(\alpha)-E_0\right]=0,\qquad V(\alpha)=-\frac{q^2L_x^2}{2L_y^2}\cos(2\alpha), \tag{46}$$

where E_0 is an integration constant that depends on the boundary conditions for α. The explicit solution can be written in terms of a certain Jacobi elliptic function. The corresponding topological charge density reads

$$\rho_B=\frac{3qp\sin(qy)}{L_xL_yL_z}\partial_x(2\alpha-\sin(2\alpha)). \tag{47}$$

By considering the boundary conditions for α,

$$\alpha(2\pi)-\alpha(0)=n\pi,\qquad n\in\mathbb{Z}, \tag{48}$$

then the topological charge is given by $B=np$. Therefore, the baryon charge can be an arbitrary integer number. This solution describes stationary soliton crystals with the shape of ordered arrays of baryonic tubes carrying topological charge. Here the integer p can be interpreted as the baryonic charge per unit of length in the z direction per tube. This can be seen by looking at the energy density of the solution $\epsilon\equiv T_{00}$,

$$\epsilon=\frac{1}{2}K\left(\frac{\alpha'^2}{L_x^2}+\sin^2(\alpha)\left(\frac{q^2}{L_y^2}+\frac{2p^2\sin^2(qy)}{L_z^2}\right)\right), \tag{49}$$

which is depicted in Fig. 13.

B. Crystals with the dilaton

Here we study the effect of the dilaton on the solutions considered in the previous section. In particular, we consider U given by Eqs. (18) and (45) and we assume that the dilaton field depends only on the x coordinate, i.e., $\sigma=\sigma(x)$. Consequently, the field equations reduce to two coupled nonlinear ODEs for $\alpha(x)$ and $\sigma(x)$,

$$\alpha''-2f\alpha'\sigma'-\frac{L_x^2}{2L_y^2}q^2\sin(2\alpha)-L_x^2m_\pi^2\sin(\alpha)e^{-f(y-2)\sigma}=0, \tag{50}$$

$$\sigma''+fK\alpha'^2-f\sigma'^2+\frac{L_x^2}{L_y^2}fKq^2\sin^2(\alpha)-L_x^2e^{2f\sigma}\partial_\sigma V(\sigma) - KfL_x^2m_\pi^2y\cos(\alpha)e^{-f(y-2)\sigma}=0. \tag{51}$$

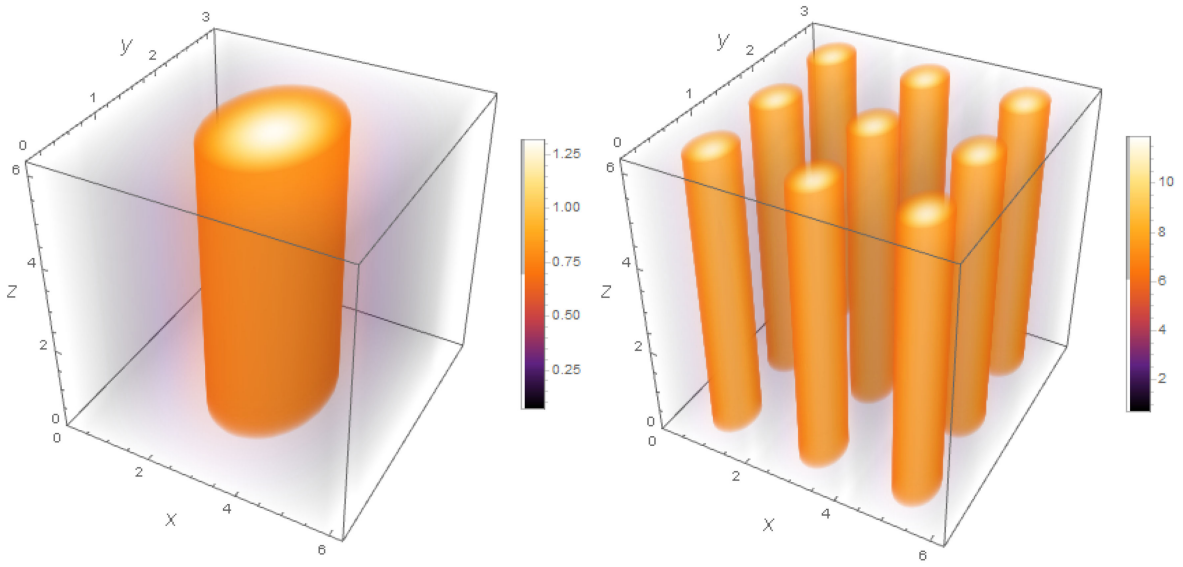

FIG. 13. Energy density of the solution (46) for $p = q = n = 1$ (left) and $p = q = n = 3$ (right). In both cases, we have assumed $K = L_x = L_z = 1$ and $L_y = 2$.

The topological charge is given by Eq. (47), while the energy density evaluated on this ansatz reads

$$\epsilon = \frac{1}{2}Ke^{-2f\sigma}\left(\sin^2(\alpha)\left(\frac{q^2}{L_y^2}+\frac{2p^2\sin^2(qy)}{L_z^2}\right)+\frac{\alpha'^2}{L_x^2}\right) + \frac{e^{-2f\sigma}\sigma'^2}{2L_x^2} - Km_\pi^2\cos(\alpha)e^{-fy\sigma}+V(\sigma) \tag{52}$$

and reduces to Eq. (49) for $\sigma = m_\pi = 0$. We proceed by focusing on the massless case $m_\pi = m_\sigma = 0$, which unlike the massive case can be partially addressed analytically. In fact, it is quite remarkable that, at the special parameter point $f^2K = 1$, the field equations (50) and (51) can be reduced to a system of first order ODEs given by

$$\alpha' = q\cos(\alpha), \qquad \sigma' = -\frac{q}{f}\sin(\alpha), \tag{53}$$

where for the sake of simplicity we have chosen $L_x = L_y$. This can also be seen by noting that the EOMs (50) and (51) coincide with the EOMs (31) and (32) for the hedgehog ansatz up to a constant term $\frac{1}{4f}$ in Eq. (32). The latter shifts the special combination of parameters from $f^2K = 7/8$ to $f^2K = 1$ reducing the second order equations of motion to the above set of first order ones, yielding the solutions

$$\alpha(x) = 2\arctan\left(\tanh\left(\frac{1}{2}(c_1+qx)\right)\right), \tag{54}$$

$$\sigma(x) = -\frac{1}{f}\left[c_2+2\operatorname{arctanh}\left(\tanh^2\left(\frac{1}{2}(c_1+qx)\right)\right)\right], \tag{55}$$

where c_1 and c_2 are the integration constants. The behavior of these solutions is shown in Fig. 14. We can restore all the integration constants stemming from the second order original EOMs and write the solution as

$$\alpha(x) = n\pi + \arctan\left(d_1e^{qx}+d_2e^{-qx}\right), \qquad n\in\mathbb{Z}, \tag{56}$$

$$\sigma(x) = -\frac{1}{f}\left(c_2+\frac{1}{2}\log\left((d_1e^{qx}+d_2e^{-qx})^2+1\right)\right). \tag{57}$$

When the parameter p is an integer it is possible to have an integer topological charge B only by considering a box that has an infinite length in the x direction. In such a case we have $B = p$, but the total energy carried by the solution diverges. This is in net contrast with the solution in the absence of the dilaton field, where for $p\in\mathbb{Z}$ one can confine an arbitrary amount of topological charge in a finite-size box and the corresponding energy is finite. On the other hand, we can relax the condition $p\in\mathbb{Z}$ and determine the value of p such that a certain amount of topological charge is confined in a finite-size box. Without losing generality, we consider $0 \le x \le 2\pi$ and impose BCs $\alpha(0) = 0$ and $\alpha(2\pi) = s$ with $0 < s < \pi/2$. The topological charge reads

$$B = -2\int_{\alpha(0)}^{\alpha(2\pi)}\frac{p}{\pi}\sin^2(\alpha)d\alpha. \tag{58}$$

Hence $B\in\mathbb{Z}$ can be achieved when

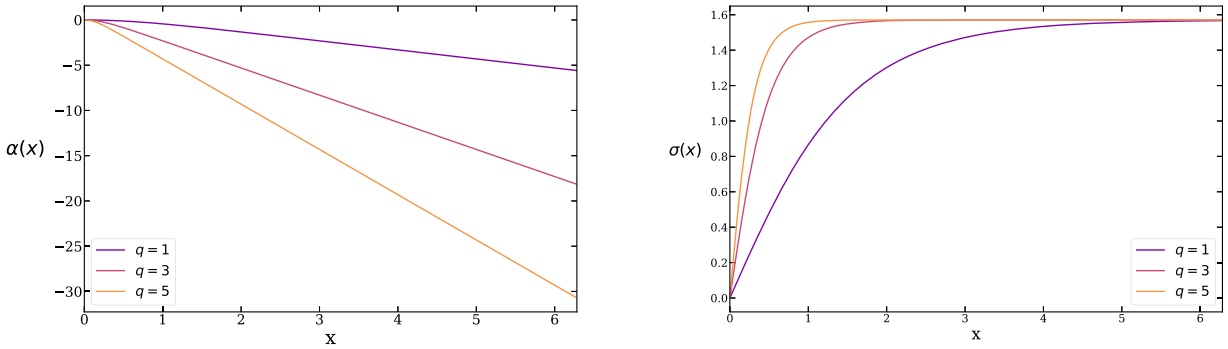

FIG. 14. The profiles $\alpha(x)$ (left) and $\sigma(x)$ (right) for $q = 1, 3, 5$.

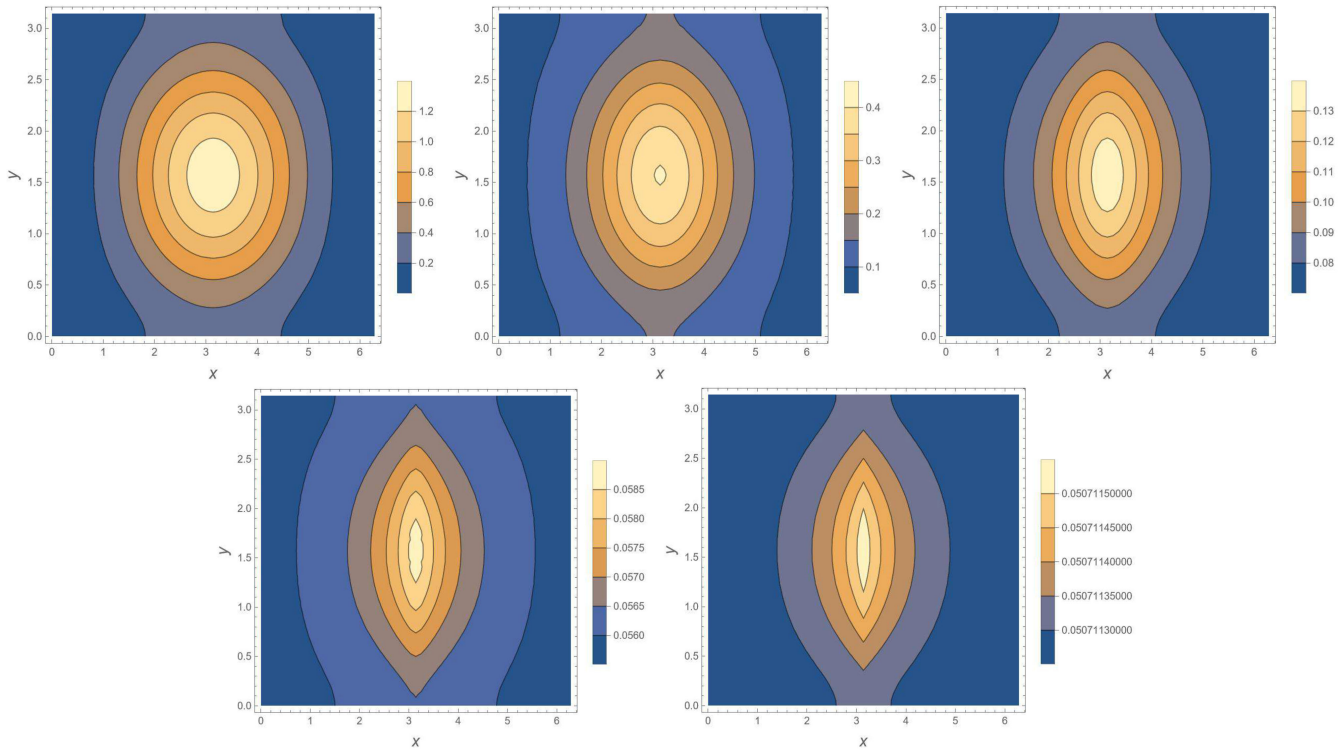

FIG. 15. Contour plot of the energy density in the $x - y$ plane for $m_\pi = m_\sigma = 0$ varying $X = f^2K$. From left to right and top to bottom we have $X = 0, 0.3, 0.6, 0.9, 1$. As X goes from 0 to 1 the results interpolate between the analytical solution found in [74–77] in the absence of the dilaton field and the solution (54).

$$p = \frac{2\pi B}{\sin(2s) - 2s}. \tag{59}$$

We conclude this section by numerically investigating the behavior of the solution for different values of $X \equiv f^2K$. The corresponding energy density is shown in Fig. 15. At $X = 0$ the EOMs decouple; the dilaton solution is $\sigma(x) = c_1 - \log(c_2 + x)$, $\{c_1, c_2\} \in \mathbb{R}$, while $\alpha(x)$ solves Eq. (46) yielding a field configuration with localized energy and integer topological charge. On the other hand, for $X = 1$ we have the analytical solution (54), whose energy grows indefinitely for increasing x. The physical impact of this solution will be discussed below.

C. Stability analysis

In this section, we consider a nontrivial test of the stability of the crystal solutions in the presence of the dilaton. In many situations when the hedgehog property holds, i.e., the equations of motion reduce to a single equation for the soliton profile, the most "dangerous" perturbations are those that keep the structure of the ansatz since they are likely to lead to a lower-energy state [103,104]. In the presence of the dilaton, these perturbations are of the following form:

$$\alpha = \alpha_0(r) + \varepsilon u(r), \tag{60}$$

$$\sigma = \sigma_0(r) + \varepsilon v(r), \tag{61}$$

where α_0 and σ_0 solve Eq. (53) and $0 \leq \varepsilon \ll 1$. These perturbations do not involve the isospin degrees of freedom Θ and Φ. A straightforward computation shows that the linearized EOMs for $u(r)$ and $v(r)$ always have a zero mode $u(r) = \nabla_r \alpha_0(r)$ and $v(r) = \nabla_r \sigma_0(r)$. The contribution of this configuration to the density energy is given by

$$\delta E = \frac{2Kq}{L^2} \varepsilon e^{-2f\sigma_0(r)} \sin(\alpha_0(r))(p^2 \sin^2(\theta q) + q^2) \geq 0. \quad (62)$$

Therefore, the present solutions are stable under the above potentially dangerous perturbations.

D. Isospin-charge separation

A further intriguing feature of the effective chiral Lagrangian dressed with the dilaton is the following. In the solutions without dilaton [74–77], the peaks corresponding to the local maxima of the topological charge density are in the same locations as the peaks corresponding to the local maxima of the isospin charge density (as one can also check via a direct computation). On the other hand, the isospin current [which is the Noether current associated with the $SU(2)$ isospin rotations of the theory] is deformed by the presence of the dilaton, while the definition of the topological charge density does not change (being the usual baryon charge). This implies that the local maxima of these two relevant quantities no longer coincide. Indeed, by setting for simplicity $L_x = L_y = L_z \equiv L$, the topological charge density reads

$$\rho_B = \frac{12pq}{L^3} \sin(yq) \alpha'(x) \sin^2(\alpha(x)), \quad (63)$$

while the isospin charge density is

$$\rho_I = K \mathrm{Tr}(R^0 \tau_3) e^{-2f\sigma(x)} = \frac{2Kp}{L} e^{-2f\sigma(x)} \sin^2(yq) \sin^2(\alpha(x)). \quad (64)$$

In Fig. 16 we compare the two charge densities to illustrate the different positions of the peaks.

This "separation" of the peaks of baryonic and isospin charge densities could open the interesting possibility of defining the analog of the well-known phenomenon in condensed matter physics called spin-charge separation (see, e.g., [94,95] and references therein). In the condensed matter version of this phenomenon, due to the presence of strong correlations, spin and charge may cease to be tied generating independent branches of excitations. In the present case, it could be possible to observe isospin-baryon charge separation thanks to the presence of the dilaton which can support excitations that change directly the isospin and only indirectly the baryon charge density.

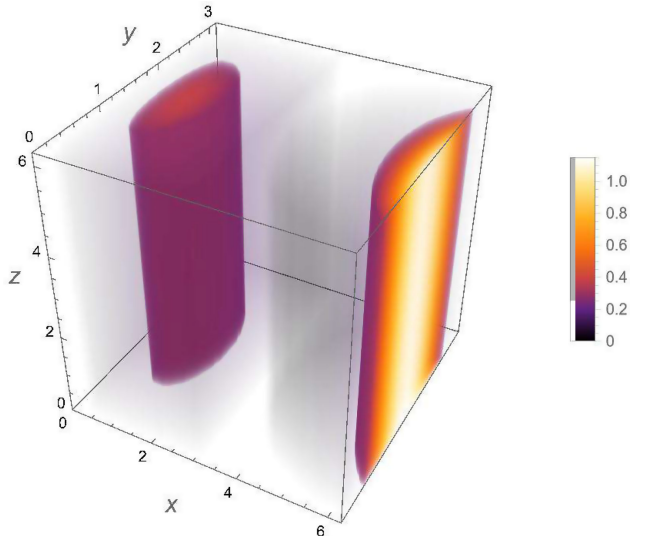

FIG. 16. Topological- (left) and isospin- (right) charge densities for $L = B = q = 1$ and $\alpha(2\pi) = s = \frac{\pi}{4}$.

V. DILATON AUGMENTED BRANES

In [70–73,77], another family of analytical solutions of the massless chiral Lagrangian has been discovered. These are again obtained by confining the theory in a box according to the metric equation (43) and considering the following ansatz:

$$U = e^{\frac{1}{2}py\tau_3} e^{\frac{1}{4}x\tau_2} e^{\frac{1}{2}\tau_3 F(t,z)}, \quad p \in \mathbb{Z}. \quad (65)$$

The above represents a particular instance of Euler angle parametrization for $SU(2)$ which implies the following range for x and y [105,106]:

$$0 \leq y \leq \pi, \quad 0 \leq x \leq 2\pi. \quad (66)$$

Without losing generality, we can also consider

$$0 \leq z \leq 2\pi. \quad (67)$$

The topological charge density is given by

$$\rho_B = \frac{3p}{4L_x L_y L_z} \sin\left(\frac{x}{2}\right) \partial_z F. \quad (68)$$

The periodicity of physical observables along with the properties of the Euler angles parametrization fixes the boundary condition satisfied by $F(t,z)$ as

$$F(t, z=0) - F(t, z=2\pi) = \pm 8\pi q, \quad q \in \mathbb{Z}. \quad (69)$$

As a consequence, the topological charge reads

$$B = -\frac{p}{8\pi} \left(F(t, z=0) - F(t, z=2\pi)\right) = pq. \quad (70)$$

Noticeably, for $m_\pi = 0$ the EOMs (5) evaluated on the ansatz (65) reduce to the field equation of a free massless scalar in $d = 2$ dimensions [73],

$$\left(\partial_t^2 - \frac{1}{L_z^2}\partial_z^2\right) F(t,z) = 0. \tag{71}$$

The general solution to the previous equations can be decomposed as the sum of two independent modes $F = F_+\left(\frac{t}{L_z} + z\right) + F_-\left(\frac{t}{L_z} - z\right)$. The latter can be generically written using the following representation:

$$F_+ = z_+^0 + v_+\left(\frac{t}{L_z} + z\right) + \sum_{n\neq 0}\left(a_n^+ \sin\left[n\left(\frac{t}{L_z} + z\right)\right] + b_n^+ \cos\left[n\left(\frac{t}{L_z} + z\right)\right]\right), \tag{72}$$

$$F_- = z_-^0 + v_-\left(\frac{t}{L_z} - z\right) + \sum_{n\neq 0}\left(a_n^- \sin\left[n\left(\frac{t}{L_z} - z\right)\right] + b_n^- \cos\left[n\left(\frac{t}{L_z} - z\right)\right]\right), \tag{73}$$

with coefficients $z_\pm^0, v_\pm, a_n^\pm, b_n^\pm$. In this way, the topological charge (70) is nonzero when $v_+ - v_- \neq 0$. Additionally, the coefficients $v_\pm$ have to be chosen such that

$$F(t, z=0) = z_+^0 + z_-^0 + (v_+ + v_-)\frac{t}{L_z} \quad \Rightarrow \quad v_+ + v_- = 0, \tag{74}$$

$$F(t, z=2\pi) = z_+^0 + z_-^0 + (v_+ - v_-)2\pi \quad \Rightarrow \quad v_+ - v_- = 4q. \tag{75}$$

The energy density of the solution reads

$$\epsilon = \frac{K}{8}\left[\frac{1}{4}\left(\frac{1}{L_x^2} + \frac{4p^2}{L_y^2}\right) + (\partial_t F)^2 + \frac{1}{L_z^2}(\partial_z F)^2\right] \tag{76}$$

and is illustrated in Fig. 17. One can see that this solution describes modulated layers of nuclear matter.

The inclusion of the Skyrme term yields an additional equation

$$(\partial_t F)^2 - \frac{1}{L_z^2}(\partial_z F)^2 = \left(\partial_t F - \frac{1}{L_z}\partial_z F\right)\left(\partial_t F + \frac{1}{L_z}\partial_z F\right) = 0, \tag{77}$$

with solution $F(t,z) = F\left(z \pm \frac{t}{L_z}\right)$. On the other hand, the equations of motion do not admit any solution of the form (65) when $m_\pi \neq 0$.

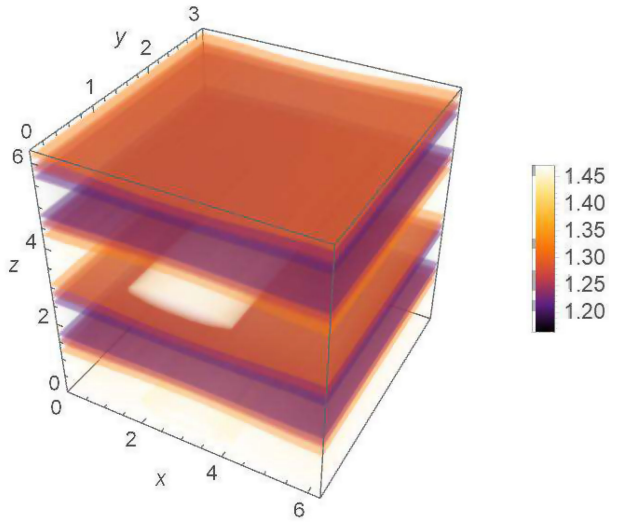

FIG. 17. Energy density of a solution of the EOMs (71) exhibiting a layer structure. We choose $F = F_+\left(\frac{t}{L_z} + z\right) = \cos\left(\frac{t}{L_z} + z\right)$.

Equipped with the above, we now investigate the impact of the dilaton on this class of topologically nontrivial solutions of the chiral and Skyrme models in the chiral limit $m_\pi = 0$. Assuming $\sigma = \sigma(t,z)$, the EOMs are

$$\partial_t^2 F - \frac{1}{L_z^2}\partial_z^2 F = 0, \tag{78}$$

$$(\partial_t F)^2 - \frac{1}{L_z^2}(\partial_z F)^2 = 0, \tag{79}$$

$$\partial_z F \partial_z \sigma - L_z^2 \partial_t F \partial_t \sigma = 0, \tag{80}$$

$$\partial_t^2\sigma - \frac{1}{L_z^2}\partial_z^2\sigma - f\left((\partial_t\sigma)^2 - \frac{1}{L_z^2}(\partial_z\sigma)^2\right) - \frac{fk}{16}\left(\frac{4p^2}{L_y^2} + \frac{1}{L_x^2}\right) + e^{2f\sigma}\partial_\sigma V(\sigma) = 0. \tag{81}$$

The baryon charge does not depend on the dilaton and, therefore, it is still given by Eq. (70). The energy density reads

$$\begin{aligned}\varepsilon = {} & \frac{K e^{-2f\sigma}(4L_x^2L_y^2(L_z^2\partial_t F^2 + \partial_z F^2) + L_z^2(L_y^2 + 4L_z^2p^2))}{32L_x^2L_y^2L_z^2} \\ & + \frac{e^{-2f\sigma}(L_z^2\partial_t\sigma^2 + \partial_z\sigma^2)}{2L_z^2} \\ & + \frac{\lambda K((L_z^2\partial_t F^2 + \partial_z F^2)(L_y^2 + 4L_x^2p^2\sin^2(\frac{r}{2})) + L_z^2p^2)}{128L_x^2L_y^2L_z^2} \\ & + V(\sigma).\end{aligned} \tag{82}$$

A. Branes in the conformal limit

We start by setting to zero both the Skyrme term and the dilaton potential. In this case, the EOMs for the brane ansatz (65) admits an analytical solution carrying topological charge where the U and σ fields are, respectively, static and homogeneous. It reads

$$F(z) = c_1 + c_2 z, \qquad \sigma(t) = \frac{1}{f}\left\{ d_1 - \log\left| \cos\left(\frac{\sqrt{K}\sqrt{4c_2^2 L_y^2 L_x^2 + L_z^2(L_y^2 + 4L_x^2 p^2)}(d_2 + ft)}{4L_y L_x L_z} \right) \right| \right\}, \tag{83}$$

where c_1, c_2, d_1, and d_2 are arbitrary integration constants. The boundary conditions (69) for $F(z)$ impose $c_2 = 4q$, whereas the energy density evaluated on the solution is both homogeneous and static,

$$\epsilon = \frac{K}{32 L_y^2 L_x^2 L_z^2} e^{-2d_1}[L_y^2(64 L_x^2 q^2 + L_z^2) + 4L_x^2 L_z^2 p^2]. \tag{84}$$

Moreover, since the U field is static, the isospin charge density of this solution vanishes identically. The time evolution of the dilaton field is depicted in Fig. 18. Note that this solution is nonanalytic in time due to a series of branch-cut singularities lying at

$$ft = \frac{2L_y L_x L_z \pi(2n+1)}{\sqrt{K}\sqrt{L_y^2(64L_x^2 q^2 + L_z^2) + 4L_x^2 L_z^2 p^2}} - d_2, \qquad n \in \mathbb{Z}. \tag{85}$$

It is possible to construct another analytical solution to the EOMs of the massless chiral Lagrangian where, akin to the case without the dilaton, $F(z,t)$ can be expressed as a particular linear combination of left- and right-moving modes

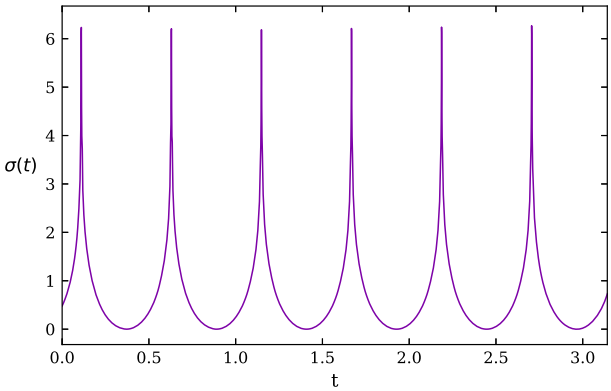

FIG. 18. Time evolution of the dilaton solution (83).

$$F(t,z) = c_1 + c_2\left[\left(z + \frac{t}{L_z}\right) - A\left(z - \frac{t}{L_z}\right)\right],$$
$$\frac{\sigma(t,z)}{\sqrt{k}} = d_1 + d_2\left[\left(z + \frac{t}{L_z}\right) + A\left(z - \frac{t}{L_z}\right)\right], \tag{86}$$

where

$$A = \frac{L_z^2(L_y^2 + 4L_x^2 p^2)}{16 L_l^2 L_x^2 (c_2^2 + 4d_2^2)}. \tag{87}$$

However, for $d_2 \neq 0$ the energy of this solution either grows or decays exponentially in time depending on the boundary conditions. Noticeably, when $d_2 = 0$ the solution for the dilaton is a constant and the energy of the solution is exactly twice that of (84).

There are no nontrivial solutions with U given by Eq. (65) for $m_\pi \neq 0$. Moreover, when $m_\sigma = 0$ there are no solutions of the EOMs when adding the Skyrme term together with dilatonic dynamics. However, as we will see in the next section, for nonvanishing dilaton mass we have been able to find analytical solutions with the ansatz (65) including the Skyrme term.

B. Branes in the near-conformal Skyrme model

Our goal in this section is to study the most general solution of the EOMs (78) of the dilaton augmented Skyrme model including the Skyrme term. This is of the form

$$F(t,z) \equiv F\left(\frac{t}{L_z} \pm z\right), \qquad \sigma(t,z) = c, \tag{88}$$

where for a dilaton potential of the form (10) the dilaton vacuum expectation value (VEV) c is determined by the following equation:

$$\chi_0^{\Delta-2} + \frac{\beta(\Delta-4)}{m_\sigma^2} - \chi_0^2 = 0, \qquad \chi_0 \equiv e^{-cf}, \tag{89}$$

where

$$\beta = \frac{1}{16} f^2 K \left(\frac{4p^2}{L_y^2} + \frac{1}{L_x^2} \right). \tag{90}$$

The properties of the soliton affect the dilaton VEV through the value of the parameter p which is related to the topological charge via Eq. (70). For $m_\sigma \to \infty$, the solution is $c = 0$. On the other hand, when $\Delta \to 4$ or $m_\sigma \to 0$ the VEV becomes undetermined since the potential vanishes. In the special cases $\Delta \to 0, 4$ and $\Delta = 2$ the dilaton VEV reads

$$2fc = \begin{cases} \sinh^{-1}\left(\frac{2\beta}{m_\sigma^2}\right) & \Delta \to 0 \\ -\log\left(1 - \frac{2\beta}{m_\sigma^2}\right) & \Delta = 2 \\ -W\left(-\frac{2\beta}{m_\sigma^2}\right) & \Delta \to 4, \end{cases} \tag{91}$$

where $W(x)$ denotes the Lambert W function. Only in the $\Delta = 0$ case is c real for arbitrary values of the dilaton mass. For $\Delta = 2$ the VEV exhibits a branch-cut singularity at $m_\sigma^2 = 2\beta$ and the solution is complex for smaller masses. Analogously, in the $\Delta \to 4$ case the solution is real only for $m_\sigma^2 > 2e\beta$.

The energy density carried by the solution for a generic Δ is

$$\begin{aligned} \epsilon = {} & \frac{K}{32} e^{-2cf} \left(\frac{8F'\left(\frac{t}{L_z} + \phi\right)^2}{L_z^2} + \frac{4p^2}{L_y^2} + \frac{1}{L_x^2} \right) \\ & + \frac{K\lambda\left(2F'\left(\frac{t}{L_z} + \phi\right)^2 \left(L_y^2 + 4L_x^2 p^2 \sin^2\left(\frac{r}{2}\right)\right) + L_z^2 p^2\right)}{128 L_x^2 L_y^2 L_z^2} \\ & + V(c). \end{aligned} \tag{92}$$

As shown in Fig. 19, this solution describes ordered layers of matter analogous to the case without dilaton previously described. The dilaton VEV suppresses the energy density of the U field while adding a homogeneous contribution proportional to m_σ^2. As a consequence, the overall effect of the dilaton is to smooth out the layer structure.

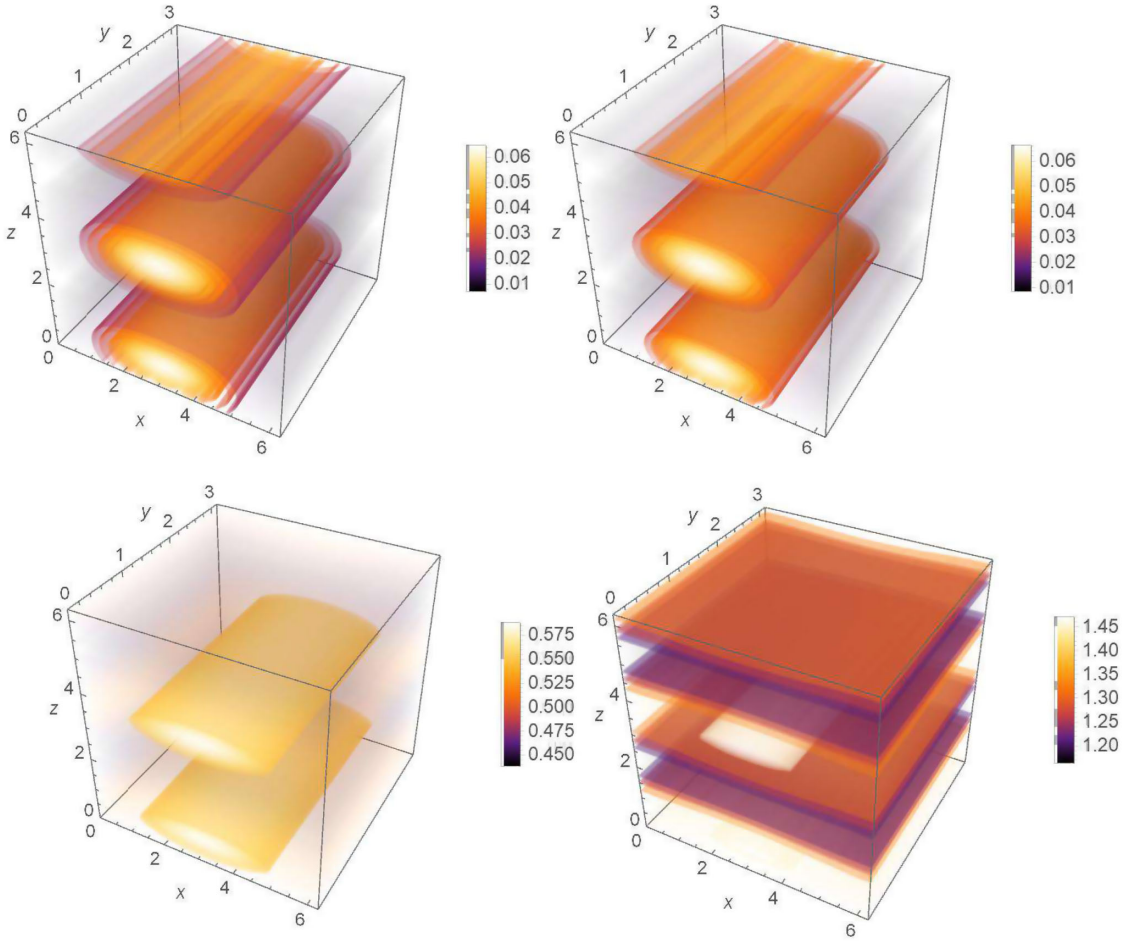

FIG. 19. Energy density of the solution (88) for $\Delta \to 0$ and different values of the dilaton mass. We consider $m_\sigma/\sqrt{K} = 0.001$ (top-left), 0.05 (top-right), 1 (bottom-left), and 20000 (bottom-right). As we increase m_σ the dilaton decouples from the dynamics as can be seen by comparing the $m_\sigma/\sqrt{K} = 20000$ case to Fig. 17. We choose $F\left(\frac{t}{L_z} + z\right) = \cos\left(\frac{t}{L_z} + z\right)$.

Analogous solutions exist in the absence of the Skyrme term. In fact, we can now look for solutions of the form

$$F(t,z) \equiv F_+\left(\frac{t}{L_z}+z\right)+F_-\left(\frac{t}{L_z}-z\right), \quad \sigma(t,z)=c. \tag{93}$$

Note that, different from Eq. (88), this is not the most general solution to the EOM. By plugging the above into the EOMs (78) with $\lambda = 0$ we have

$$fKL_z^2(L_y^2+4L_x^2p^2) - 16L_y^2L_x^2\left[L_z^2e^{2cf}\frac{\partial V(\sigma)}{\partial\sigma}\bigg|_{\sigma=c} - fKF'_+\left(\frac{t}{L_z}+\phi\right)F'_-\left(\phi-\frac{t}{L_z}\right)\right]=0, \tag{94}$$

which admits solutions if and only if

(1) either F_+ or F_- vanishes;
(2) both F_+ and F_- are linear functions of their argument.

In the first case, the solution is equal to the one in the presence of the Skyrme term with the dilaton VEV given by Eq. (89). In the second case, we have

$$F(t,z) = a_0 + a_1\left(\frac{t}{L_z}+\phi\right)+a_2\left(\frac{t}{L_z}-\phi\right), \tag{95}$$

and the dilaton VEV is again determined by Eq. (89) with β now given by

$$\beta = \frac{f^2K(16a_1a_2L_y^2L_x^2+L_z^2(L_y^2+4L_x^2p^2))}{16L_y^2L_x^2L_z^2}. \tag{96}$$

For $m_\sigma = 0$ this reduces to the solution (86) with $d_2 = 0$.

VI. CONCLUSIONS

We fused numerical and analytical methods to perform a thorough investigation of skyrmion solutions featuring dilatonic dynamics. Employing the dilaton-dressed chiral Lagrangian we addressed the impact on relevant physical quantities such as the traditional skyrmion profile, mass, and size stemming from varying the near-conformal controlling parameters. We discovered an intriguing dependence of these physical properties on the dilaton mass. A notable result is the observation of a quick dilaton decoupling once its mass surpasses the pion one. The decoupling is further enhanced at large values of the anomalous dimension of the chiral condensate. Another interesting feature is the occurrence of a special value of the ratio of the dilaton to pion decay constants where the coupled second order field equations of the dilaton augmented EFT reduce to a first order solvable system. In this case, one arrives at analytic solitonic solutions even though this phenomenon is not related to a BPS bound. The resulting special solutions have negative topological charge $B = -1$ and are singular at the origin. Because in several instances in the literature, nuclear matter, at the core of compact stars, has been argued to feature near-conformal dynamics [80,86–88], we employed QCD-inspired values of the parameters to represent our findings. Our setup can be further extended to investigate face-centered-cubic skyrmion crystals featuring dilaton dynamics which provide a description of nuclear matter and its equation of state [107,108].

We further presented the impact of dilatonic dynamics on skyrmion crystals and have identified a special parameter point, linked to the case of the traditional skyrmion above, for which the second order differential equations also reduces to a set of first order ones. Here another observed feature, stemming from the presence of the dilaton, is that the latter spatially separates the baryon and isospin charge distributions similar to the spin-charge separation phenomenon.

Additionally, we considered dilaton-modified solitonic branes and showed that the soliton profile is unaltered by the presence of the dilaton while the latter acquires a homogeneous vacuum expectation value. We have also shown how the dilaton smooths out the brane configurations. One of the original appeals of the brane solutions, without the dilaton, is that they can be analytically derived from the equations of motion. Our results show that it is still possible to obtain analytic solutions in the presence of dilaton dynamics. Attempts to connect brane solutions to phenomenological applications were discussed in [73] where the authors compared the thermodynamic properties of the solutions to lattice QCD calculations.

More generally, our results have broad implications ranging from the near-conformal dynamics of QCD-like theories to nuclear matter in extreme regimes. For example, for the near-conformal dynamics in vacuum, one can now compare our results to the ones from lattice investigations of the nucleon spectrum close to the lower end of the conformal window.

ACKNOWLEDGMENTS

We are indebted to Fabrizio Canfora for a fruitful collaboration at the early stage of the project and precious suggestions. M. T. was supported by Agencia Nacional de Investigación y Desarrollo (ANID) Grant No. 7221039. The work of J. B. was supported by the World Premier International Research Center Initiative (WPI Initiative), MEXT, Japan and also supported in part by the JSPS KAKENHI Grant No. JP23K19047. The work of F. S. is partially supported by the Carlsberg Foundation, Grant No. CF22-0922.

APPENDIX: TABLES OF THE SKYRMION MASS AND THE ROOT-MEAN-SQUARE RADIUS OF THE BARYON CHARGE

In this appendix, we list in a series of tables our results for the skyrmion mass M_S and the root-mean-square radius

of the baryon charge $\langle r^2\rangle^{1/2}$ in the single spherical skyrmion case studied in Sec. III. We estimated an error not larger than the 0.5% for all the entries. All the dimensionful quantities are measured in units of $\sqrt{K}$. $M_{\text{Skyrme}} = 15.67$ and $\langle r^2\rangle^{1/2}_{\text{Skyrme}} = 0.215$ denote the skyrmion mass and the root-mean-square radius in the absence of the dilaton, respectively.

1. General case

2. M_S and $\langle r^2\rangle^{1/2}$ in the $\Delta \to 0$ limit

TABLE I. Numerical values of the skyrmion mass for different values of the conformal dimension Δ and dilaton mass $m_\sigma = 1$–5. $M_{\text{Skyrme}} = 15.67$ denotes the skyrmion mass in the absence of the dilaton.

Skyrmion mass										
	M_S					M_S/M_{Skyrme}				
Δ	$m_\sigma = 1$	$m_\sigma = 2$	$m_\sigma = 3$	$m_\sigma = 4$	$m_\sigma = 5$	$m_\sigma = 1$	$m_\sigma = 2$	$m_\sigma = 3$	$m_\sigma = 4$	$m_\sigma = 5$
1	22.58	16.28	15.43	15.26	15.24	1.46	1.04	0.985	0.974	0.973
1.2	22.27	16.26	15.43	15.26	15.24	1.44	1.04	0.985	0.974	0.972
1.4	21.98	16.24	15.43	15.26	15.24	1.42	1.04	0.984	0.973	0.972
1.6	21.71	16.23	15.42	15.25	15.24	1.40	1.04	0.984	0.973	0.972
1.8	21.46	16.21	15.42	15.25	15.24	1.39	1.03	0.984	0.973	0.972
2	21.22	16.19	15.42	15.25	15.23	1.37	1.03	0.984	0.973	0.972
2.2	21.00	16.18	15.41	15.25	15.23	1.36	1.03	0.984	0.973	0.972
2.4	20.79	16.16	15.41	15.25	15.23	1.34	1.03	0.984	0.973	0.972
2.6	20.60	16.15	15.41	15.24	15.23	1.33	1.03	0.983	0.973	0.972
2.8	20.42	16.14	15.40	15.24	15.23	1.32	1.03	0.983	0.973	0.972
3	20.25	16.12	15.40	15.24	15.23	1.31	1.03	0.983	0.973	0.972
3.2	20.08	16.10	15.40	15.24	15.23	1.30	1.03	0.983	0.972	0.972
3.4	19.93	16.09	15.40	15.24	15.22	1.29	1.03	0.982	0.972	0.971
3.6	19.79	16.07	15.39	15.24	15.22	1.28	1.03	0.982	0.972	0.971
3.8	19.65	16.06	15.39	15.23	15.22	1.27	1.02	0.982	0.972	0.971
4	19.53	16.05	15.39	15.23	15.22	1.25	1.02	0.98	0.972	0.971

TABLE II. Numerical values of the root-mean-square radius $\langle r^2\rangle^{1/2}$ of the baryon charge for different values of the conformal dimension Δ and dilaton mass $m_\sigma = 1$–5. $\langle r^2\rangle^{1/2}_{\text{Skyrme}} = 0.215$ denotes the root-mean-square radius of the baryon charge for the Skyrme model in the absence of the dilaton.

Root-mean-square radius of the baryon charge										
	$\langle r^2\rangle^{1/2}$ in units of 10^{-1}					$\langle r^2\rangle^{1/2}/\langle r^2\rangle^{1/2}_{\text{Skyrme}}$ in units of 10^{-1}				
Δ	$m_\sigma = 1$	$m_\sigma = 2$	$m_\sigma = 3$	$m_\sigma = 4$	$m_\sigma = 5$	$m_\sigma = 1$	$m_\sigma = 2$	$m_\sigma = 3$	$m_\sigma = 4$	$m_\sigma = 5$
1	1.50	2.04	2.14	2.158	2.161	6.99	9.47	9.94	10.03	10.04
1.2	1.52	2.04	2.14	2.158	2.161	7.08	9.48	9.94	10.03	10.04
1.4	1.54	2.04	2.14	2.158	2.161	7.17	9.49	9.94	10.03	10.04
1.6	1.56	2.04	2.14	2.158	2.161	7.25	9.50	9.94	10.03	10.04
1.8	1.58	2.05	2.14	2.158	2.161	7.33	9.51	9.94	10.03	10.04
2	1.60	2.05	2.14	2.159	2.161	7.43	9.52	9.95	10.03	10.04
2.2	1.61	2.05	2.14	2.159	2.161	7.50	9.53	9.95	10.03	10.04
2.4	1.63	2.05	2.14	2.159	2.161	7.57	9.54	9.95	10.03	10.05
2.6	1.64	2.05	2.14	2.159	2.161	7.64	9.54	9.95	10.03	10.05
2.8	1.66	2.06	2.14	2.159	2.162	7.70	9.55	9.95	10.04	10.05
3	1.67	2.06	2.14	2.159	2.162	7.76	9.56	9.95	10.04	10.05
3.2	1.68	2.06	2.14	2.160	2.162	7.82	9.57	9.96	10.04	10.05
3.4	1.70	2.06	2.14	2.160	2.162	7.88	9.57	9.96	10.04	10.05
3.6	1.71	2.06	2.14	2.160	2.162	7.93	9.58	9.96	10.04	10.05
3.8	1.72	2.06	2.14	2.160	2.162	7.98	9.59	9.96	10.04	10.05
4	1.73	2.07	2.14	2.160	2.162	8.05	9.61	9.96	10.04	10.05

TABLE III. Numerical values of the skyrmion mass for different values of the conformal dimension Δ and dilaton mass $m_\sigma = 6$–10. $M_{\text{Skyrme}} = 15.67$ denotes the skyrmion mass in the absence of the dilaton.

Skyrmion mass										
	M_S					M_S/M_{Skyrme}				
Δ	$m_\sigma = 6$	$m_\sigma = 7$	$m_\sigma = 8$	$m_\sigma = 9$	$m_\sigma = 10$	$m_\sigma = 6$	$m_\sigma = 7$	$m_\sigma = 8$	$m_\sigma = 9$	$m_\sigma = 10$
1	15.27	15.31	15.35	15.38	15.41	0.974	0.977	0.979	0.982	0.984
1.2	15.27	15.31	15.35	15.38	15.41	0.974	0.977	0.979	0.981	0.984
1.4	15.27	15.30	15.34	15.38	15.41	0.974	0.977	0.979	0.981	0.984
1.6	15.26	15.30	15.34	15.38	15.41	0.974	0.976	0.974	0.981	0.983
1.8	15.26	15.30	15.34	15.38	15.41	0.974	0.976	0.979	0.981	0.983
2	15.26	15.30	15.34	15.38	15.41	0.974	0.976	0.979	0.981	0.983
2.2	15.26	15.30	15.34	15.38	15.41	0.974	0.976	0.979	0.981	0.983
2.4	15.26	15.30	15.34	15.38	15.41	0.974	0.976	0.979	0.981	0.983
2.6	15.26	15.30	15.34	15.38	15.41	0.974	0.976	0.979	0.981	0.983
2.8	15.26	15.30	15.34	15.37	15.41	0.974	0.976	0.979	0.981	0.983
3	15.26	15.30	15.34	15.37	15.41	0.973	0.976	0.979	0.981	0.983
3.2	15.25	15.29	15.34	15.37	15.41	0.973	0.976	0.979	0.981	0.983
3.4	15.25	15.29	15.33	15.37	15.41	0.973	0.976	0.978	0.981	0.983
3.6	15.25	15.29	15.33	15.37	15.41	0.973	0.976	0.978	0.981	0.983
3.8	15.25	15.29	15.33	15.37	15.40	0.973	0.976	0.978	0.981	0.983
4	15.25	15.29	15.33	15.37	15.40	0.973	0.976	0.978	0.981	0.983

TABLE IV. Numerical values of the root-mean-square radius $\langle r^2\rangle^{1/2}$ of the baryon charge for different values of the conformal dimension Δ and dilaton mass $m_\sigma = 6$–10. $\langle r^2\rangle^{1/2}_{\text{Skyrme}} = 0.215$ denotes the root-mean-square radius of the baryon charge for the Skyrme model in the absence of the dilaton.

Root-mean-square radius of the baryon charge										
	$\langle r^2\rangle^{1/2}$ in units of 10^{-1}					$\langle r^2\rangle^{1/2}/\langle r^2\rangle^{1/2}_{\text{Skyrme}}$ in units of 10^{-1}				
Δ	$m_\sigma = 6$	$m_\sigma = 7$	$m_\sigma = 8$	$m_\sigma = 9$	$m_\sigma = 10$	$m_\sigma = 6$	$m_\sigma = 7$	$m_\sigma = 8$	$m_\sigma = 9$	$m_\sigma = 10$
1	2.160	2.159	2.159	2.159	2.159	1.004	1.004	1.003	1.003	1.003
1.2	2.160	2.159	2.159	2.159	2.159	1.004	1.004	1.003	1.003	1.003
1.4	2.160	2.159	2.159	2.159	2.159	1.004	1.004	1.003	1.003	1.003
1.6	2.160	2.159	2.159	2.158	2.159	1.004	1.004	1.003	1.003	1.003
1.8	2.160	2.159	2.159	2.158	2.159	1.004	1.003	1.003	1.003	1.003
2	2.160	2.159	2.158	2.158	2.159	1.004	1.003	1.003	1.003	1.003
2.2	2.160	2.159	2.158	2.158	2.159	1.004	1.003	1.003	1.003	1.003
2.4	2.160	2.159	2.158	2.158	2.159	1.004	1.003	1.003	1.003	1.003
2.6	2.160	2.159	2.158	2.158	2.159	1.004	1.003	1.003	1.003	1.003
2.8	2.160	2.159	2.158	2.158	2.159	1.004	1.003	1.003	1.003	1.003
3	2.160	2.159	2.158	2.158	2.158	1.004	1.003	1.003	1.003	1.003
3.2	2.160	2.159	2.158	2.158	2.158	1.004	1.003	1.003	1.003	1.003
3.4	2.160	2.159	2.158	2.158	2.147	1.004	1.003	1.003	1.003	1.003
3.6	2.160	2.159	1.003	2.158	2.158	1.004	1.003	1.003	1.003	1.003
3.8	2.160	2.159	2.158	2.158	2.158	1.004	1.003	1.003	1.003	1.003
4	2.160	2.159	2.158	2.158	2.158	1.004	1.003	1.003	1.003	1.003

TABLE V. Numerical values of the skyrmion mass M_S and the root-mean-square radius of the baryon charge $\langle r^2\rangle^{1/2}$ for $m_\sigma = 1$–5.

	Skyrmion mass	
	M_S	M_S/M_{Skyrme}
$m_\sigma = 1$	24.48	1.56
$m_\sigma = 2$	16.38	1.05
$m_\sigma = 3$	15.45	0.99
$m_\sigma = 4$	15.27	0.97
$m_\sigma = 5$	15.25	0.97

	Root-mean-square radius of the baryon charge	
	$\langle r^2\rangle^{1/2}$	$\langle r^2\rangle^{1/2}/\langle r^2\rangle^{1/2}_{\text{Skyrme}}$
$m_\sigma = 1$	0.140	0.65
$m_\sigma = 2$	0.203	0.94
$m_\sigma = 3$	0.214	0.99
$m_\sigma = 4$	0.216	1.00
$m_\sigma = 5$	0.216	1.00

TABLE VI. Numerical values of the skyrmion mass and the root-mean-square radius $\langle r^2\rangle^{1/2}$ of the baryon charge for different values of the dilaton mass measured in units of $\sqrt{K}$.

	Skyrmion mass	
	M_S	M_S/M_{Skyrme}
$m_\sigma = 6$	15.27	0.974
$m_\sigma = 7$	15.31	0.977
$m_\sigma = 8$	15.35	0.980
$m_\sigma = 9$	15.39	0.982
$m_\sigma = 10$	15.42	0.984

	Root-mean-square radius of the baryon charge	
	$\langle r^2\rangle^{1/2}$	$\langle r^2\rangle^{1/2}/\langle r^2\rangle^{1/2}_{\text{Skyrme}}$
$m_\sigma = 6$	0.216	1.004
$m_\sigma = 7$	0.216	1.004
$m_\sigma = 8$	0.216	1.003
$m_\sigma = 9$	0.216	1.003
$m_\sigma = 10$	0.216	1.004

[1] T. H. R. Skyrme, A nonlinear field theory, Proc. R. Soc. A **260**, 127 (1961).

[2] Gregory S. Adkins, Chiara R. Nappi, and Edward Witten, Static properties of nucleons in the Skyrme model, Nucl. Phys. **B228**, 552 (1983).

[3] Gregory S. Adkins and Chiara R. Nappi, The Skyrme model with pion masses, Nucl. Phys. **B233**, 109 (1984).

[4] Gregory S. Adkins and Chiara R. Nappi, Stabilization of chiral solitons via vector mesons, Phys. Lett. **137B**, 251 (1984).

[5] I. Zahed and G. E. Brown, The Skyrme model, Phys. Rep. **142**, 1 (1986).

[6] P. Jain, R. Johnson, Ulf G. Meissner, N. W. Park, and J. Schechter, Realistic pseudoscalar vector chiral Lagrangian and its soliton excitations, Phys. Rev. D **37**, 3252 (1988).

[7] Ulf G. Meissner, Low-energy hadron physics from effective chiral Lagrangians with vector mesons, Phys. Rep. **161**, 213 (1988).

[8] William Detmold, Christoph Lehner, and Stefan Meinel, $\Lambda_b \to p\ell^-\bar{\nu}_\ell$ and $\Lambda_b \to \Lambda_c\ell^-\bar{\nu}_\ell$ form factors from lattice QCD with relativistic heavy quarks, Phys. Rev. D **92**, 034503 (2015).

[9] Dante Bigi and Paolo Gambino, Revisiting $B \to D\ell\nu$, Phys. Rev. D **94**, 094008 (2016).

[10] Yasmine Sara Amhis *et al.*, Averages of b-hadron, c-hadron, and τ-lepton properties as of 2021, Phys. Rev. D **107**, 052008 (2023).

[11] Curtis G. Callan, Jr. and Igor R. Klebanov, Bound state approach to strangeness in the Skyrme model, Nucl. Phys. **B262**, 365 (1985).

[12] Robert L. Jaffe, Perhaps a stable dihyperon, Phys. Rev. Lett. **38**, 195 (1977); **38**, 617(E) (1977).

[13] N. N. Scoccola, H. Nadeau, Maciej A. Nowak, and Mannque Rho, The hyperons as skyrmions with vector mesons, Phys. Lett. B **201**, 425 (1988); **220**, 658(E) (1989).

[14] David B. Kaplan and Igor R. Klebanov, The role of a massive strange quark in the large-N Skyrme model, Nucl. Phys. **B335**, 45 (1990).

[15] Y. Kondo, S. Saito, and T. Otofuji, Semileptonic hyperon decays in the Skyrme model with bound kaon approach to strangeness, Phys. Lett. B **256**, 316 (1991).

[16] H. Weigel, Reinhard Alkofer, and H. Reinhardt, Hyperons in the bound state approach to the Nambu-Jona-Lasinio chiral soliton, Nucl. Phys. **A576**, 477 (1994).

[17] E. Eichten and F. Feinberg, Spin dependent forces in QCD, Phys. Rev. D **23**, 2724 (1981).

[18] Zachary Guralnik, Michael E. Luke, and Aneesh V. Manohar, Properties of baryons containing a heavy quark in the Skyrme model, Nucl. Phys. **B390**, 474 (1993).

[19] Elizabeth Ellen Jenkins and Aneesh V. Manohar, Hyperfine splittings of baryons containing a heavy quark in the Skyrme model, Phys. Lett. B **294**, 273 (1992).

[20] Yong-seok Oh, Byung-Yoon Park, and Dong-Pil Min, Heavy baryons as Skyrmion with $\frac{1}{m_Q}$ corrections, Phys. Rev. D **49**, 4649 (1994).

[21] Kumar S. Gupta, M. Arshad Momen, J. Schechter, and A. Subbaraman, Heavy quark solitons, Phys. Rev. D **47**, R4835 (1993).

[22] J. Schechter, A. Subbaraman, S. Vaidya, and H. Weigel, Heavy quark solitons: Towards realistic masses, Nucl. Phys. **A590**, 655 (1995); **598**, 583(E) (1996).
[23] Masayasu Harada, Asif Qamar, Francesco Sannino, Joseph Schechter, and Herbert Weigel, Hyperfine splitting of low lying heavy baryons, Nucl. Phys. **A625** (1997), 789.
[24] Masayasu Harada, Francesco Sannino, Joseph Schechter, and Herbert Weigel, Generalization of the bound state model, Phys. Rev. D **56**, 4098 (1997).
[25] M. B. Voloshin and Mikhail A. Shifman, On the annihilation constants of mesons consisting of a heavy and a light quark, and $B^0 \leftrightarrow \bar{B}^{-0}$ oscillations, Sov. J. Nucl. Phys. **45**, 292 (1987).
[26] Nathan Isgur and Mark B. Wise, Weak decays of heavy mesons in the static quark approximation, Phys. Lett. B **232**, 113 (1989).
[27] Mark B. Wise, Combining chiral and heavy quark symmetry, in *CCAST Symposium on Particle Physics at the Fermi Scale* (1993), pp. 71–114. arXiv:hep-ph/9306277.
[28] Matthias Neubert, Heavy quark symmetry, Phys. Rep. **245**, 259 (1994).
[29] Michael E. Luke and Aneesh V. Manohar, Reparametrization invariance constraints on heavy particle effective field theories, Phys. Lett. B **286**, 348 (1992).
[30] Adam F. Falk and Matthias Neubert, Second order power corrections in the heavy quark effective theory. 2. Baryon form-factors, Phys. Rev. D **47**, 2982 (1993).
[31] Adam F. Falk, Benjamin Grinstein, and Michael E. Luke, Leading mass corrections to the heavy quark effective theory, Nucl. Phys. **B357**, 185 (1991).
[32] Francesco Sannino and Kimmo Tuominen, Orientifold theory dynamics and symmetry breaking, Phys. Rev. D **71**, 051901 (2005).
[33] Dennis D. Dietrich and Francesco Sannino, Conformal window of SU(N) gauge theories with fermions in higher dimensional representations, Phys. Rev. D **75**, 085018 (2007).
[34] V. A. Miransky, Dynamics of spontaneous chiral symmetry breaking and continuum limit in quantum electrodynamics, Nuovo Cimento Soc. Ital. Fis. **90A**, 149 (1985).
[35] V. A. Miransky and Koichi Yamawaki, Conformal phase transition in gauge theories, Phys. Rev. D **55**, 5051 (1997); **56**, 3768(E) (1997).
[36] Bob Holdom, Raising condensates beyond the ladder, Phys. Lett. B **213**, 365 (1988).
[37] Bob Holdom, Continuum limit of quenched theories, Phys. Rev. Lett. **62**, 997 (1989).
[38] Andrew G. Cohen and Howard Georgi, Walking beyond the rainbow, Nucl. Phys. **B314**, 7 (1989).
[39] Steven Weinberg, Implications of dynamical symmetry breaking, Phys. Rev. D **13**, 974 (1976); **19**, 1277(E) (1979).
[40] Thomas Appelquist, P. S. Rodrigues da Silva, and Francesco Sannino, Enhanced global symmetries and the chiral phase transition, Phys. Rev. D **60**, 116007 (1999).
[41] Zhi-yong Duan, P. S. Rodrigues da Silva, and Francesco Sannino, Enhanced global symmetry constraints on epsilon terms, Nucl. Phys. **B592**, 371 (2001).
[42] Dennis D. Dietrich, Francesco Sannino, and Kimmo Tuominen, Light composite Higgs from higher representations versus electroweak precision measurements: Predictions for CERN LHC, Phys. Rev. D **72**, 055001 (2005).
[43] Giacomo Cacciapaglia, Claudio Pica, and Francesco Sannino, Fundamental composite dynamics: A review, Phys. Rep. **877**, 1 (2020).
[44] David B. Kaplan and Howard Georgi, SU(2) × U(1) Breaking by vacuum misalignment, Phys. Lett. **136B**, 183 (1984).
[45] David B. Kaplan, Howard Georgi, and Savas Dimopoulos, Composite Higgs scalars, Phys. Lett. **136B**, 187 (1984).
[46] Giacomo Cacciapaglia and Francesco Sannino, Fundamental composite (Goldstone) Higgs dynamics, J. High Energy Phys. 04 (2014) 111.
[47] Ben Gripaios, Alex Pomarol, Francesco Riva, and Javi Serra, Beyond the minimal composite Higgs model, J. High Energy Phys. 04 (2009) 070.
[48] Jamison Galloway, Jared A. Evans, Markus A. Luty, and Ruggero Altair Tacchi, Minimal conformal technicolor and precision electroweak tests, J. High Energy Phys. 10 (2010) 086.
[49] James Barnard, Tony Gherghetta, and Tirtha Sankar Ray, UV descriptions of composite Higgs models without elementary scalars, J. High Energy Phys. 02 (2014) 002.
[50] Francesco Sannino, Alessandro Strumia, Andrea Tesi, and Elena Vigiani, Fundamental partial compositeness, J. High Energy Phys. 11 (2016) 029.
[51] Domenico Orlando, Susanne Reffert, and Francesco Sannino, Charging the conformal window, Phys. Rev. D **103**, 105026 (2021).
[52] Jahmall Bersini, Alessandra D'Alise, Francesco Sannino, and Matías Torres, Charging the conformal window at nonzero θ angle, Phys. Rev. D **107**, 125024 (2023).
[53] Zackaria Chacko and Rashmish K. Mishra, Effective theory of a light dilaton, Phys. Rev. D **87**, 115006 (2013).
[54] Shinya Matsuzaki and Koichi Yamawaki, Dilaton chiral perturbation theory: Determining the mass and decay constant of the technidilaton on the lattice, Phys. Rev. Lett. **113**, 082002 (2014).
[55] Aya Kasai, Ken-ichi Okumura, and Hiroshi Suzuki, A dilaton-pion mass relation, arXiv:1609.02264.
[56] Martin Hansen, Kasper Langæble, and Francesco Sannino, Extending chiral perturbation theory with an isosinglet scalar, Phys. Rev. D **95**, 036005 (2017).
[57] Maarten Golterman and Yigal Shamir, Low-energy effective action for pions and a dilatonic meson, Phys. Rev. D **94**, 054502 (2016).
[58] Maarten Golterman and Yigal Shamir, Effective pion mass term and the trace anomaly, Phys. Rev. D **95**, 016003 (2017).
[59] Thomas Appelquist, James Ingoldby, and Maurizio Piai, Dilaton EFT framework for lattice data, J. High Energy Phys. 07 (2017) 035.
[60] Maarten Golterman and Yigal Shamir, Large-mass regime of the dilaton-pion low-energy effective theory, Phys. Rev. D **98**, 056025 (2018).
[61] Oscar Catá and Christoph Müller, Chiral effective theories with a light scalar at one loop, Nucl. Phys. **B952**, 114938 (2020).

[62] Maarten Golterman, Ethan T. Neil, and Yigal Shamir, Application of dilaton chiral perturbation theory to $N_f = 8$, SU(3) spectral data, Phys. Rev. D **102**, 034515 (2020).
[63] Thomas Appelquist, James Ingoldby, and Maurizio Piai, Nearly conformal composite Higgs model, Phys. Rev. Lett. **126**, 191804 (2021).
[64] Maarten Golterman and Yigal Shamir, Dilaton chiral perturbation theory and applications, Proc. Sci. LATTICE2021 (**2022**) 372 [arXiv:2110.07930].
[65] Thomas Appelquist, James Ingoldby, and Maurizio Piai, Dilaton effective field theory, Universe **9**, 10 (2023).
[66] Thomas Appelquist, James Ingoldby, and Maurizio Piai, Dilaton potential and lattice data, Phys. Rev. D **101**, 075025 (2020).
[67] R. J. Crewther and Lewis C. Tunstall, $\Delta I = 1/2$ rule for kaon decays derived from QCD infrared fixed point, Phys. Rev. D **91**, 034016 (2015).
[68] O. Catá, R. J. Crewther, and Lewis C. Tunstall, Crawling technicolor, Phys. Rev. D **100**, 095007 (2019).
[69] Roman Zwicky, QCD with an infrared fixed point: The pion sector, Phys. Rev. D **109**, 034009 (2024).
[70] Fabrizio Canfora, Magnetized baryonic layer and a novel BPS bound in the gauged-non-linear-sigma-model-Maxwell theory in $(3+1)$-dimensions through Hamilton-Jacobi equation, J. High Energy Phys. 11 (2023) 007.
[71] P. D. Alvarez, F. Canfora, N. Dimakis, and A. Paliathanasis, Integrability and chemical potential in the $(3+1)$-dimensional Skyrme model, Phys. Lett. B **773**, 401 (2017).
[72] Eloy Ayon-Beato, Fabrizio Canfora, and Jorge Zanelli, Analytic self-gravitating skyrmions, cosmological bounces and AdS wormholes, Phys. Lett. B **752**, 201 (2016).
[73] Fabrizio Canfora, Diego Hidalgo, Marcela Lagos, Enzo Meneses, and Aldo Vera, Infinite conformal symmetry and emergent chiral fields of topologically nontrivial configurations: From Yang-Mills-Higgs theory to the Skyrme model, Phys. Rev. D **106**, 105016 (2022).
[74] Fabrizio Canfora, Ordered arrays of baryonic tubes in the Skyrme model in $(3+1)$ dimensions at finite density, Eur. Phys. J. C **78**, 929 (2018).
[75] Gonzalo Barriga, Fabrizio Canfora, Matías Torres, and Aldo Vera, Crystals of gauged solitons, force free plasma and resurgence, Phys. Rev. D **103**, 096023 (2021).
[76] Gonzalo Barriga, Fabrizio Canfora, Marcela Lagos, Matías Torres, and Aldo Vera, On the robustness of solitons crystals in the Skyrme model, Nucl. Phys. **B983**, 115913 (2022).
[77] Fabrizio Canfora and Scarlett C. Rebolledo-Caceres, Skyrmions at finite density, Mod. Phys. Lett. A **38**, 2330002 (2023).
[78] Hee-Jung Lee, Byung-Yoon Park, Mannque Rho, and Vicente Vento, Sliding vacua in dense skyrmion matter, Nucl. Phys. **A726**, 69 (2003).
[79] Byung-Yoon Park, Mannque Rho, and Vicente Vento, The role of the dilaton in dense skyrmion matter, Nucl. Phys. **A807**, 28 (2008).
[80] Yong-Liang Ma and Mannque Rho, Pseudoconformal structure in dense baryonic matter, Phys. Rev. D **99**, 014034 (2019).
[81] Long-Qi Shao and Yong-Liang Ma, Scale symmetry and composition of compact star matter, Phys. Rev. D **106**, 014014 (2022).
[82] Won-Gi Paeng, Thomas T. S. Kuo, Hyun Kyu Lee, Yong-Liang Ma, and Mannque Rho, Scaleinvariant hidden local symmetry, topology change, and dense baryonic matter. II, Phys. Rev. D **96**, 014031 (2017).
[83] G. E. Brown and Mannque Rho, On the manifestation of chiral symmetry in nuclei and dense nuclear matter, Phys. Rep. **363**, 85 (2002).
[84] Jeremy W. Holt, Mannque Rho, and Wolfram Weise, Chiral symmetry and effective field theories for hadronic, nuclear and stellar matter, Phys. Rep. **621**, 2 (2016).
[85] Yong-Liang Ma, Masayasu Harada, Hyun Kyu Lee, Yongseok Oh, Byung-Yoon Park, and Mannque Rho, Dense baryonic matter in the hidden local symmetry approach: Half-skyrmions and nucleon mass, Phys. Rev. D **88**, 014016 (2013); **88**, 079904(E) (2013).
[86] Won-Gi Paeng, Thomas T. S. Kuo, Hyun Kyu Lee, and Mannque Rho, Scale-invariant hidden local symmetry, topology change and dense baryonic matter, Phys. Rev. C **93**, 055203 (2016).
[87] Yuki Fujimoto, Kenji Fukushima, Larry D. McLerran, and Michal Praszalowicz, Trace anomaly as signature of conformality in neutron stars, Phys. Rev. Lett. **129**, 252702 (2022).
[88] Michael Marczenko, Larry McLerran, Krzysztof Redlich, and Chihiro Sasaki, Reaching percolation and conformal limits in neutron stars, Phys. Rev. C **107**, 025802 (2023).
[89] G. E. Brown and Mannque Rho, Scaling effective Lagrangians in a dense medium, Phys. Rev. Lett. **66**, 2720 (1991).
[90] M. Harada, F. Sannino, J. Schechter, and H. Weigel, Scaling behavior in soliton models, Phys. Lett. B **384**, 5 (1996).
[91] Yan-Ling Li, Yong-Liang Ma, and Mannque Rho, Chiral-scale effective theory including a dilatonic meson, Phys. Rev. D **95**, 114011 (2017).
[92] Yong-Liang Ma and Wen-Cong Yang, Topology and emergent symmetries in dense compact star matter, Symmetry **15**, 776 (2023).
[93] Yong-Liang Ma and Mannque Rho, Topology change, emergent symmetries and compact star matter, AAPPS Bull. **31**, 16 (2021).
[94] Feng He, Yu-Zhu Jiang, Hai-Qing Lin, Randall G. Hulet, Han Pu, and Xi-Wen Guan, Emergence and disruption of spin-charge separation in one-dimensional repulsive fermions, Phys. Rev. Lett. **125**, 190401 (2020).
[95] Alberto Lerda, A field theory approach to the $t-J$ model and the spin charge separation, Nucl. Phys. **B428**, 629 (1994).
[96] D. G. Ravenhall, C. J. Pethick, and J. R. Wilson, Structure of matter below nuclear saturation density, Phys. Rev. Lett. **50**, 2066 (1983).
[97] Jorge A. Lopez, Claudio O. Dorso, and Guillermo A. Frank, Properties of nuclear pastas, Front. Phys. (Beijing) **16**, 24301 (2021).
[98] Sidney Coleman, *Aspects of Symmetry: Selected Erice Lectures* (Cambridge University Press, Cambridge, England, 1988).

[99] Walter D. Goldberger, Benjamin Grinstein, and Witold Skiba, Distinguishing the Higgs boson from the dilaton at the Large Hadron Collider, Phys. Rev. Lett. **100**, 111802 (2008).
[100] Riccardo Rattazzi and Alberto Zaffaroni, Comments on the holographic picture of the Randall-Sundrum model, J. High Energy Phys. 04 (2001) 021.
[101] Zackaria Chacko and Rashmish K. Mishra, Effective theory of a light dilaton, Phys. Rev. D **87**, 115006 (2013).
[102] Roman Zwicky, QCD with an infrared fixed point and a dilaton, Phys. Rev. D **110**, 014048 (2024).
[103] Mikhail Shifman and Alexei Yung, *Supersymmetric Solitons*, Cambridge Monographs on Mathematical Physics (Cambridge University Press, Cambridge, England, 2023).
[104] Mikhail Shifman, *Advanced Topics in Quantum Field Theory: A Lecture Course* (Cambridge University Press, Cambridge, England, 2012).
[105] Stefan Bertini, S. L. Cacciatori, and Bianca L. Cerchiai, On the Euler angles for SU(N), J. Math. Phys. (N.Y.) **47**, 043510 (2006).
[106] S. L. Cacciatori, F. Dalla Piazza, and A. Scotti, Compact Lie groups: Euler constructions and generalized Dyson conjecture, Trans. Am. Math. Soc. **369**, 4709 (2017).
[107] M. Kugler and S. Shtrikman, Skyrmion crystals and their symmetries, Phys. Rev. D **40**, 3421 (1989).
[108] Yong-Liang Ma and Masayasu Harada, Lecture notes on the Skyrme model, arXiv:1604.04850.